University of California
Los Angeles

Immersed boundary method for coupled fluid-structure interaction problems

A thesis submitted in partial satisfaction
of the requirements for the degree
Master of Science in Aerospace Engineering

by

Amaury Bannier

2012

Abstract of the Thesis

Immersed boundary method for coupled fluid-structure interaction problems

by

Amaury Bannier

Master of Science in Aerospace Engineering

University of California, Los Angeles, 2012

Professor Jeffrey D. Eldredge, Chair

A new fluid-structure interaction approach for bio-inspired regime is presented. In this method, the incompressible fluid flow is discretized using the fast immersed boundary method with nullspace approach, previously developed by Colonius and Taira [CT08]. The Lagrangian solid dynamics solver is greatly inspired from the virtual node algorithm by Zhu *et al.* [ZWH12]. The two system are coupled to satisfy the physical constraints at their interface.

A new weak formulation of the immersed boundary method coherently enforces the interface force balance and the no-slip condition. Boundary stresses are treated as Lagrange multipliers to maintain a strong coupling. Strongly coupled solver are known to handle problems on which weakly coupled methods encounter stability restrictions (problems including large density ratio for instance).

Numerical simulations have been conducted to model the vibrations of an initially perturbed elastic disk immersed in a fluid. Results have shown an inconsistency in the enforcement of the boundary stress term on the fluid system. Accuracy and convergence of the solid and the fluid solvers have been evaluated.

The thesis of Amaury Bannier is approved.

Joseph M. Teran

William S. Klug

Jeffrey D. Eldredge, Committee Chair

University of California, Los Angeles

2012

[...] Vous pouvez tourner le dos à demain et vivre hier,
ou vous pouvez être heureux demain parce qu'il y a eu hier [...]

Eileen Cicole, *L'ultime adieu*

Table of Contents

List of Figures

List of Tables

Acknowledgments

My time spent at UCLA would not have been the same if Professor Jeff Eldredge had not trusted me enough to give me a chance. A chance to supplement my knowledge. A chance to experience scholarly research. A chance to fulfill my curiosity... and arouse it even more! I would like to express my sincere gratitude for his guidance and his patience.

Thank you to Professor Tim Colonius and Professor Joseph Teran, who not only inspired this thesis through their respective publications [CT08, ZWH12] but also shared invaluable opinions and advice. I also want to acknowledge Professor Jeff Eldredge, Professor Joseph Teran and Professor William Klug for serving as members of my thesis review committee.

Finally, I would like to express how thankful I am to my family and to my friends who made this year an incredible academic, social, cultural and personal adventure. My last and deepest thought goes to the contagious enthusiasm and the memorable smile of my friend Antoine. Mate, you rocked my world!

CHAPTER 1

Introduction

Fluid-structure interaction (FSI) is a key phenomenon in the understanding of numerous biological systems. A common example is the locomotion of flying and swimming animals: from insects to birds, from flagellate bacteria to marine mammals. The challenge in those systems lies in the coupling of highly flexible structure with the surrounding fluid. To understand and be able to mimic, with engineered devices, those complex systems, one must be able to efficiently simulate the tight coupling between the fluid and the structure. Cardiovascular or laryngeal flows are examples of medical applications where modeling FSI would greatly contribute to the development of pathology treatments.

A suitable solver should be able to deal with two fundamentally different governing equations on either side of a complex and moving boundary, and solve them simultaneously, such that both the kinematic and the dynamic boundary conditions are enforced at their interface.

An easy tracking of the moving interface would be possible with a Lagrangian description of the fluid. However, the mesh distortion often prevents the use of this method. The two main alternatives are particles methods and Eulerian grid-based methods. A class of particles methods are the Vortex Methods [Leo80] on which is based the Viscous Vortex Particles Methods (VVPM) [CK00]. The Navier-stokes equation is solved using Lagrangian particles of vorticity, advected and diffused by the flow. Gingold and Monaghan introduced the Smoothed Particle Hydrodynamics [GM77]. By discretizing the velocity-pressure formulation of the compressible Navier-Stokes equation, they avoid having to solve for the velocity by an elliptic problem. Those methods have already been used for fluid-body interactions

problems [Eld08, HK08]. Indeed, they are inherently capable of handling flows past complex and deforming geometries, since particle attributes describing the flow are advected with it. However, when particles are diffused, a re-meshing is needed and the interpolation of the old strength distribution to the new locations leads to inherent leakage errors.

Discretization on an Eulerian frame is another widely used technique for simulating fluid. In particular, unstructured grids [FL93] such as standard body-fitted meshes offer a straightforward way for enforcing accurately boundary conditions if the interface lies along meshlines, even for complex boundaries. On the other hand, differential equations become more complicated to differentiate and, in the case of moving boundaries, the new grid generation leads to an expensive computational cost and extra interpolation errors [HPZ01, JH04].

Based on the VVPM introduced by Chorin [Cho73], Peskin developed the pioneering Immersed Boundary Method (IBM) [Pes72] for simulating FSI of heart valves. In the IBM, governing equations are discretized on an Eulerian (usually Cartesian) grid. Since the boundary is not conformed by the mesh, its influence is accounted for by a singular forcing term. The ease for grid generation, for multigrid approaches and for fast Fourier transform techniques are the main advantages of the IBM [CT08]. Diverse variants, such as the Immersed Interface Methods [LL94, LL97], are described in the review by Mittal and Iaccarino [MI05]. Those variants can be categorized between sharp- and diffuse- interface methods. Sharp methods are able to accurately solve the flow close to boundary, but the spatial discretization scheme has to be modified when the boundary is moving. Diffuse methods, on the contrary, cannot solve accurately in the immediate vicinity of the boundary, but deal more easily with the border motions.

Although Finite Element Method (FEM) are also used to describe a fluid within the general framework of the IBMs [WL04, LLF06], our method is based on the Eulerian finite volume formulation by Taira and Colonius [TC07] where no-slip condition and incompressiblility are enforced through a projection. In this diffuse-interface method [MI05], a singular boundary force is smeared at the interface location to enforce the boundary constraints, providing the flexibility to efficiently handle moving boundary. A fast sine transform technique

[CT08] is employed to boost the solving of the linear system.

On the solid side, the use of a Lagrangian description is advantageous: it greatly simplifies the treatment of history-dependent material laws. Moreover, the solid boundary location does not need to be updated, by definition, in the reference state formulation. However, the Lagrangian approach is not essential: the Reference Map Technique [KRN12] is an example of such Eulerian treatment for finite-strain elastic solid in large deformation. Nevertheless, Lagrangian approach for structure modeling appears to be a simpler choice. As we will see, the coupling of an Eulerian fluid a Lagrangian structure can be handle without too many difficulties. In fact, the original formulation by Peskin [Pes72] was already one of those nowadays extensively used [UMR01, LCB06, LMZ08, WB09, GKF11] Eulerian-Lagrangian FSI methods [Ben92].

As mentioned above with the fluid, the same duality between body-conforming but unstructured grid on one hand, and structured (Cartesian) grid which does not fit the boundary on the other hand, exists for the structure discretization. The traditional choice in solid dynamics goes for FEM on a structured grid, by virtue of its ease of dealing with complicated computational domain [BM00]. However, the Immersed Boundary methods defined earlier has also been applied to the computation of solid dynamics. Sethian and Wiegmann [SW00] took advantages of it for the optimization of an elastic structure design without generating expensive body-conforming mesh at each iteration. More recently, Zhu *et al.* developed a cut-cell method for static simulations of loaded linear elastic material [ZWH12]. This sharp-interface method has been the foundation of the dynamics structure solver used in our FSI method. Virtual nodes on cut uniform Cartesian grid cells provide the geometric flexibility in the domain boundary shape without sacrificing accuracy. The use of a structured grid should be also considered as a strong advantage regarding the possible future modification of the algorithm to be handle by parallel computing.

A key feature of our current method is the strong coupling between the two materials. By

coupling, one should understand an equating of particular variables at the interface of the two subsystems: boundary velocity and stress for instance. In numerical implementations, one can equate these variables by enforcing one subsystem to match the values given by the other one. Luo *et al.* [LMZ08] compute the two, fluid and structure, subsystems sequentially: the flow is computed one time-step ahead with the prescribed velocity boundary condition imposed by the solid structure. From this computation, new fluid boundary stresses are applied on the structure to move it one step ahead and update new velocity boundary conditions for the next fluid time-step, and so on. This weak coupling has been shown to give accurate results [FAM99, Fed02] but suffers from poor stability restrictions (on fluid-solid density ratios [CGN05] for example). By improving the estimate of the interface values, this issue can be alleviated, as shown by Liu *et al.* [LKX06]. Implementation of a strongly coupled system enables us to totally avoid this instability issue. To implicitly match interface conditions, the variables to equate must be treated as additional interface unknowns and solved alongside structure-related and fluid-related unknowns. Previous works have been conducted successfully on FSI problems involving both incompressible [Pes02, RSG08] or compressible flows [GKF11]. Wang & Belytschko [WB09] treat the FSI coupling terms in a strong way, evaluating the boundary traction implicitly by a backward Euler method.

Our formulation conveys the physical coupling of the system all along the discretization process. The fluid will be treated by an Eulerian description taken from [TC07] and [CT08] while the solid solver is built on a Lagrangian framework greatly inspired from [ZWH12]. By its Lagrangian nature, the Finite Element structure code does not involve substantial matrix update time-step after time-step to accommodate from the potentially large deformation. However, the location of the interface is determined accurately by use of a doubly-refined grid sharp boundary method. On the other side, the Finite Volume fluid method takes advantages of the incompressibility of the flow through a projection onto the vorticity nullspace, which drastically reduces the dimension of the linear system. A flow is solved on the whole computational domain, such that the Fast Fourier Transform techniques can be used to efficiently

solve Poisson's equation on a uniform Cartesian grid. Appropriate boundary conditions are enforced at the interface between the actual flow field and the solid domain (where a fictitious flow is also computed). To be consistent with the solid FEM, the enforcement is a weak formulation of the usual IBMs. Thus, weighted integrations of velocity and stress along elemental boundary segments are carried out with both the fluid and the solid in order to enforce their matching. Following the process of numerous diffuse-interface IBMs, a discrete delta function is used to transfer information from the fluid grid to the boundary locations. This spatial discretization allows for the writing of a coupled ordinary differential system. A single Newmark time-marching scheme is applied to the global system, and the resulting coupled equation is solved with the Fractional Step Method [Per93].

In the following section, the methodology will be explained: the general assumptions are stated in the part 2.1. The solid and fluid spatial discretization are developed in 2.2 and 2.3 respectively. The time-marching scheme and the solving procedure of the global coupled system are explained in 2.4 and 2.5. The ability of the method will be demonstrated in section 3.

CHAPTER 2

Methodology

Obtaining of versatile code, able to model, in a strongly coupled way, an elastic solid structure interacting with the surrounding incompressible flow has been the target of this study.

The fluid-structure interaction system is sketched on Figure 2.1. The superscript F refers to the fluid, while the superscript S refers to the solid structure.

Ω is the global computational domain and Ω^F and Ω^S are the fluid and the solid domains respectively. The two latter constitute a partition of Ω and are thus disjointed: $\Omega^F \cap \Omega^S = \emptyset$. Nevertheless, due to the immersed boundary method used here, a fluid flow is computed in the whole domain $\Omega = \Omega^F \cup \Omega^S$. Indeed, as will be developed in section 2.3, a fictitious flow is solved in the structure domain Ω^S.

Γ^{FSI} denotes the fluid-structure interaction interface lying between Ω^F and Ω^S. This boundary is defined implicitly by a signed distance function. Γ^F_τ and Γ^S_τ are the natural boundaries (subject to Neumann boundary conditions) and Γ^F_v and Γ^S_v, the essential boundaries (subject to Dirichlet boundary conditions).

Because the structure is treated within the Lagrangian framework, its governing equations will referred to material coordinates $\underline{X}$. As for the fluid, spatial coordinates $\underline{x}$ are preferred for an Eulerian approach.

The solid structure is subject to movement and deformation. Hence, material properties and previously defined domains may be time-dependant. We use a naught subscript to denote the reference state, by opposition to the current state: reference solid domain Ω^S_0 versus current domain $\Omega^S(t)$, initial reference density $\rho^S_0(\underline{X})$ versus current density $\rho^S(\underline{X}, t)$, and

also reference coordinates gradient $\nabla_0 = \dfrac{\partial}{\partial \underline{X}}$ versus current coordinates gradient $\nabla = \dfrac{\partial}{\partial \underline{x}}$.

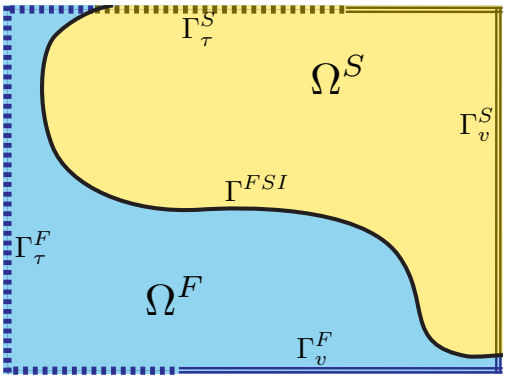

Figure 2.1: *General fluid-structure interaction system. The fluid domain Ω^F is depicted in blue, the solid domain Ω^S in yellow. Natural boundaries Γ_τ are represented by a dotted line, and essential boundaries Γ_v by a doubled line. The fluid-structure interface is the plain black line.*

2.1 General assumptions and governing equations

The fluid is stated to be Newtonian and incompressible. It is characterized by its density ρ^F and its viscosity μ^F.

Incompressibility is enforced on the velocity field $\underline{u}$ by equation (2.1) and the Cauchy stress tensor $\underline{\underline{\sigma}}$ is defined by the Newtonian law (2.2). p^F is the pressure field and ∇^s refers to the symmetric part of the gradient operator: $\nabla^s \underline{u} = \frac{1}{2}\left(\nabla \underline{u} + (\nabla \underline{u})^T\right)$

$$\nabla \cdot \underline{u}(\underline{x}, t) = 0 \qquad \text{in } \Omega^F \tag{2.1}$$

$$\underline{\underline{\sigma}}(\underline{x}, t) = 2\mu^F \ \nabla^s \underline{u}(\underline{x}, t) - p^F(\underline{x}, t)\ \underline{\underline{I}} \qquad \text{in } \Omega^F \tag{2.2}$$

The solid material is considered as homogeneous, isotropic and elastic. Under the small deformation hypothesis (i.e. $\|\nabla_0 \underline{\xi}\| \ll 1$) and with no pre-stress, the Piola stress tensor $\underline{\underline{P}}$ is linearly related to the displacement $\underline{\xi}$ and the pressure p^S by the two Lamé's coefficients

μ^S and λ^S (note that the fluid viscosity μ^F and the solid shear modulus μ^S represent totally different quantities which does not even have the same dimension):

$$\underline{\underline{P}}(\underline{X},t) = 2\mu^S \ \nabla_0^s \ \underline{\xi}(\underline{X},t) \ - p^S(\underline{X},t) \ \underline{\underline{I}} \qquad \text{in } \Omega_0^S \tag{2.3}$$

$$\text{with} \qquad p^S(\underline{X},t) = -\lambda^S \ \nabla_0 \cdot \underline{\xi}(\underline{X},t) \qquad \text{in } \Omega_0^S \tag{2.4}$$

The density field, ρ^S, is linked to the reference density, ρ_0^S, by: $\rho^S J = \rho_0^S$, where J is the Jacobian determinant: $J = \det(\nabla_0 \ \underline{x}) = \det\left(\ \underline{\underline{I}} + \nabla_0 \ \underline{\xi}\ \right)$. Under the previously assumed small deformation hypothesis, one can obtain: $J = 1 + \mathrm{Tr}\left(\nabla_0 \underline{\xi}\right) + O(\|\nabla_0 \underline{\xi}\|^2)$. At first order, the incompressibility constraint for the solid ($\rho^S = \rho_0^S \Leftrightarrow J = 1 \Leftrightarrow \nabla \cdot \underline{\xi} = 0$) can be approximate if necessary by:

$$\nabla_0 \cdot \underline{\xi} = 0 \quad \Leftrightarrow \quad \lambda^S = +\infty \ \text{ in } \ (2.4) \tag{2.5}$$

The temporal evolution of variables $\underline{u}$ and $\underline{\xi}$ is given by the following momentum equations, where $\underline{b}$ denotes possible body forces, and D_t represents the material time derivative.

$$\rho^F \ D_t \underline{u}(\underline{x},t) = \nabla \cdot \underline{\underline{\sigma}} + \rho^F \underline{b}^F \qquad \text{in } \Omega^F \tag{2.6}$$

$$\rho_0^S \ D_{tt}^2 \underline{\xi}(\underline{X},t) = \nabla_0 \cdot \underline{\underline{P}} + \rho_0^S \underline{b}_0^S \qquad \text{in } \Omega_0^S \tag{2.7}$$

Denote by $\underline{n}$ the unit vector locally normal to the surface. Boundary conditions on the domain borders are:

$$\underline{\underline{\sigma}} \cdot \underline{n} = \underline{\tau}_N^F \qquad \text{on } \Gamma_\tau^F \tag{2.8}$$

$$\underline{\underline{P}} \cdot \underline{n_0} = \underline{\tau}_{N0}^S \qquad \text{on } \Gamma_{0\tau}^S \tag{2.9}$$

$$\underline{u} = \underline{u}_D \qquad \text{on } \Gamma_v^F \tag{2.10}$$

$$\underline{\xi} = \underline{\xi}_D \qquad \text{on } \Gamma_{0v}^S \tag{2.11}$$

At the fluid-structure interface Γ^{FSI}, the force balance and the no-slip condition state:

$$\underline{\underline{\sigma}} \cdot \underline{n}^{F\to S} = \ -\ \underline{\tau} \qquad \text{on } \Gamma^{FSI} \tag{2.12}$$

$$\underline{\underline{\sigma}}^S \cdot \underline{n}^{S\to F} = \quad \underline{\tau} \qquad \text{on } \Gamma^{FSI} \tag{2.13}$$

$$\underline{u}(\underline{x},t) = \ \dot{\underline{\xi}}(\underline{X},t) \qquad \text{on } \Gamma^{FSI} \tag{2.14}$$

2.1.1 Non-dimensionalization

Denote by L the length of the solid, defined as characteristic length to obtain dimensionless spatial quantities. Suppose a characteristic flow speed U_0 is given, such as a prescribed inlet velocity. The temporal quantity $t_0 = L/U_0$ appears to be a natural choice for the characteristic time.

Structure variables ($\underline{\underline{P}}$, $\underline{\tau}^S_{N0}$, p^S, μ^S and λ^S) are compared to the characteristic quantity $\rho^S_0\ U^2_0$, while fluid variables, ($\underline{\underline{\sigma}}$, $\underline{\tau}^F_N$ and p^F) are non-dimensionalized by the fluid density related quantity $\rho^F U^2_0$. For the fluid-structure interaction stress $\underline{\tau}$, we decide to use $\rho^S_0 U^2_0$ rather than $\rho^F U^2_0$. This way, the two sets of equations, fluid and solid, are specified independently from one each other. Only the velocity and stress terms at their common boundary relate the intrinsic coupling.

Define the Reynolds number Re and denote by $\tilde{\rho}^S_0$ the solid-fluid density ratio. The four dimensionless parameters of the problem are:

$$Re = \frac{\rho^F L U_0}{\mu^F} \qquad \tilde{\rho}^S_0 = \frac{\rho^S_0}{\rho^F} \qquad \tilde{\mu}^S = \frac{\mu^S}{\rho^S_0\ U^2_0} \qquad \tilde{\lambda}^S = \frac{\lambda^S}{\rho^S_0\ U^2_0} \tag{2.15}$$

Note that, in the remaining part of the document, all quantities are dimensionless and tilde signs are dropped unambiguously.

2.1.2 Strong formulation

After non-dimensionalization, we obtain a strong formulation for the governing equations.

- Continuity equations:

$$\nabla \cdot \underline{u}(\underline{x}, t) = \ 0 \qquad \text{in } \Omega^F \tag{2.16}$$

$$\nabla_0 \cdot \underline{\xi}(\underline{X}, t) = -\frac{p^S}{\lambda^S} \qquad \text{in } \Omega^S_0 \tag{2.17}$$

- Momentum equations:

$$\partial_t \underline{u} + (\underline{u} \cdot \nabla)\ \underline{u} = -\nabla p^F + \frac{1}{Re}\nabla^2 \underline{u} + \underline{b}^F \qquad \text{in } \Omega^F \tag{2.18}$$

$$\ddot{\underline{\xi}} = -\nabla p^S + \mu^S \left[\nabla_0^2 \underline{\xi} + \nabla_0(\nabla_0 \cdot \underline{\xi})\right] + \underline{b}_0^S \qquad \text{in } \Omega_0^S \tag{2.19}$$

- Boundary Conditions:

$$\underline{\underline{\sigma}} \cdot \underline{n} = \underline{\tau}_N^F \qquad \text{on } \Gamma_\tau^F \tag{2.20}$$

$$\underline{\underline{P}} \cdot \underline{n_0} = \underline{\tau}_{N0}^S \qquad \text{on } \Gamma_{0\tau}^S \tag{2.21}$$

$$\underline{u} = \underline{u}_D \qquad \text{on } \Gamma_v^F \tag{2.22}$$

$$\underline{\xi} = \underline{\xi}_D \qquad \text{on } \Gamma_{0v}^S \tag{2.23}$$

$$\underline{\underline{\sigma}} \cdot \underline{n}^{F\to S} = -\rho_0^S\ \underline{\tau} \qquad \text{on } \Gamma^{FSI} \tag{2.24}$$

$$\underline{\underline{\sigma}}^S \cdot \underline{n}^{S\to F} = \underline{\tau} \qquad \text{on } \Gamma^{FSI} \tag{2.25}$$

$$\underline{u}(\underline{x}, t) = \dot{\underline{\xi}}(\underline{X}, t) \qquad \text{on } \Gamma^{FSI} \tag{2.26}$$

The structure-related and fluid-related systems of equations are coupled only through the boundary conditions (2.24)-(2.26). The linear discretized system of equations we will obtain should retain this dependence.

2.2 Structure modeling: cut-cell finite-element method

A natural choice for the computation of solid equations is the finite element method on a body-conforming mesh. However, for moving boundary, the difficult and time-consuming meshing process of complex geometries would have to be repeated extensively.

"Embedded" methods have been developed to solve the solid motion equations on a non-body-conforming mesh. With the numerical advantages of structured Cartesian grids, second order accuracy in L^∞ has been achieved by Zhu *et al.* with their virtual node method [ZWH12] for simulating a statically loaded linear elastic structure. Their approach has been the foundation of the spatial discretization of the present solid dynamic solver. It combines piecewise bilinear interpolation of displacement components with the addition of "virtual"nodes on cut cells.

2.2.1 Weak formulation

From the momentum equation (2.19) and the boundary conditions (2.21) and (2.25), we obtain the following weak formulation (2.27). The pressure definition equation (2.17), the Dirichlet boundary condition (2.23), and the no-slip constraint at the FSI interface (2.26) lead respectively to the weak equations (2.28), (2.29), (2.30).

$$\begin{aligned}
\forall\ \delta\underline{\xi}, \qquad & \iint\limits_{\Omega_0^S} \delta\underline{\xi}\cdot\ddot{\underline{\xi}} + \iint\limits_{\Omega_0^S} 2\mu^S\ \nabla_0^s\delta\underline{\xi} : \nabla_0^s\underline{\xi} \\
& - \iint\limits_{\Omega_0^S} (\nabla_0\cdot\delta\underline{\xi})\ p^S\ - \int\limits_{\Gamma_{0v}^S} \delta\underline{\xi}\cdot\underline{\tau}_{D0}^S - \int\limits_{\Gamma^{FSI}} \delta\underline{\xi}\cdot\underline{\tau}\ = \iint\limits_{\Omega_0^S} \delta\underline{\xi}\cdot\underline{b}_0^S + \int\limits_{\Gamma_{0\tau}^S} \delta\underline{\xi}\cdot\underline{\tau}_{N0}^S \qquad (2.27)\\
\forall\ \delta p^S, \qquad & -\iint\limits_{\Omega_0^S} (\nabla_0\cdot\dot{\underline{\xi}})\ \delta p^S - \frac{1}{\lambda^S}\iint\limits_{\Omega_0^S} (\dot{p}^S\ \delta p^S) \ = \ 0 \qquad (2.28)\\
\forall\ \delta\underline{\tau}_{D0}^S, \qquad & -\int\limits_{\Gamma_{0v}^S} \dot{\underline{\xi}}\cdot\delta\underline{\tau}_{D0}^S \ = \ -\int\limits_{\Gamma_{0v}^S} \dot{\underline{\xi}}_D\cdot\delta\underline{\tau}_{D0}^S \qquad (2.29)\\
\forall\ \delta\underline{\tau}, \qquad & \int\limits_{\Gamma^{FSI}} \underline{u}\cdot\delta\underline{\tau}\ - \int\limits_{\Gamma^{FSI}} \dot{\underline{\xi}}\cdot\delta\underline{\tau} \ = \ 0 \qquad (2.30)
\end{aligned}$$

For $(\underline{\xi},\ p^S,\ \underline{\tau}^S_{D0},\ \underline{\tau}) \in H^1(\Omega_0^S)^2 \times L^2(\Omega_0^S) \times L^2(\Gamma_{0v}^S)^2 \times L^2(\Gamma^{FSI})^2$ and according to Lax-Milgram theorem, these weak formulations are equivalent to the previously stated strong forms if they can be satisfied for any arbitrary test functions $(\delta\underline{\xi},\ \delta p^S,\ \delta\underline{\tau}^S_{D0},\ \delta\underline{\tau}) \in H_0^1(\Omega_0^S)^2 \times L_0^2(\Omega_0^S) \times L^2(\Gamma_{0v}^S)^2 \times L^2(\Gamma^{FSI})^2$.

Note that the last term on the left-hand-side of equation (2.27) has been obtained using the following identity:

$$\int_{\Gamma_0^{FSI}} \underline{n}_0^{S\to F} \cdot \underline{\underline{P}} \cdot \delta\underline{\xi}\ \ d\Gamma_0 = \int_{\Gamma^{FSI}} \frac{1}{J}\ \underline{n}^{S\to F} \cdot \underline{\underline{F}} \cdot \underline{\underline{P}} \cdot \delta\underline{\xi}\ \ d\Gamma \quad \text{using:} \quad \underline{n} \cdot \underline{\underline{F}}\ d\Gamma = J\ \underline{n}_0\ d\Gamma_0 \tag{2.31}$$

$$= \int_{\Gamma^{FSI}} \underline{n}^{S\to F} \cdot \underline{\underline{\sigma}}^S \cdot \delta\underline{\xi}\ \ d\Gamma \qquad \text{using:} \qquad J\ \underline{\underline{\sigma}}^S = \underline{\underline{F}} \cdot \underline{\underline{P}} \tag{2.32}$$

$$= \int_{\Gamma^{FSI}} \underline{\tau} \cdot \delta\underline{\xi}\ d\Gamma \qquad \text{using equation (2.25)} \tag{2.33}$$

Moreover, to obtain equations (2.28) and (2.29), the strong formulation equations (2.17) and (2.23) have been differentiated in time. Although it does not affect in any way the validity of those equations, it will latter shift the matrices $\mathcal{M}^P$, ${}^t\mathcal{P}^S$ and ${}^t\mathcal{D}^S$ at the first time-derivative level in the space-discretized equation (2.41). The purpose of shifting those matrices is for the sake of simplifying the final time-discretized system which will be obtained (see (2.96)). Indeed, as it is going to be shown in section 2.4, the computed unknown vector is going to be the time-derivative $\dot{\underline{\xi}}$ of the displacement. Though, after time-discretization, the differentiated equations (2.28) and (2.29) will not involve previous time-steps.

Furthermore, the weak formulation for the pressure definition (2.28) has been divided by the Lamé's coefficient λ^S to remain valid even in the limit of an incompressible material, for which λ^S tends towards infinity. The limit equation (2.5) would then be obtained. However, as discussed in section 2.1, incompressibility for the solid is not rigorously enforced, but at first order in $\|\nabla_0\underline{\xi}\|$ under the small deformation hypothesis.

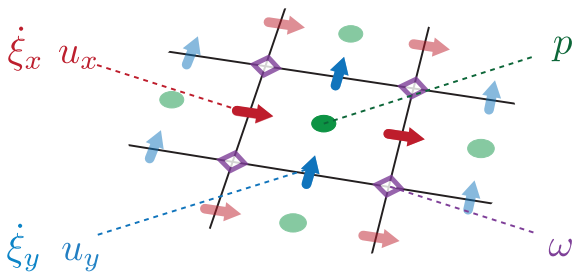

Figure 2.2: *Staggered grid discretization. The arrows represent the discrete displacement and velocity locations. Pressure is positioned at the center of each cell and vorticity at their nodes.*

2.2.2 Spatial discretization

Stability and convergence of the mixed finite element method defined on a MAC-staggered grid (Figure 2.2) have been study by [HW98] with Navier-Stokes equations. This approach has been generalized in [ZWH12] to nearly incompressible linear elasticity in embedded domain.

The solid domain, in reference state, is covered by a Lagrangian MAC-staggered square grid (Figure 2.3). Its dimensions are $n^S = n_x^S \times n_y^S$ and h_S is the discrete spacing between grid points. We will see in the next section, section 2.3, that fluid quantities are defined on an Eulerian staggered grid whose dimensions may be different.

On the MAC-staggered grid, variables locations are ordered. We equivalently denote them by their position on the grid (i, j) or by their ordered index I. Solid displacement components are known on the corresponding cell faces, so we write $\xi_{(i,j),x}$ or ξ_{Ix} the discretized values of the x-displacement of the material point initially at the locations $\underline{X} = \underline{X}_{(i,j),x} = \underline{X}_{Ix}$. The same notation is used for the y-displacement field $\xi_{(i,j),y} = \xi_{Iy}$ of points initially at $\underline{X}_{(i,j),y} = \underline{X}_{Iy}$. Similarly, the pressure field is known at the centre $\underline{X}_{(i,j),p}$ (or $\underline{X}_{Ip}$) of the cells. We note $p^S_{(i,j)}$ or p^S_I the corresponding variables.

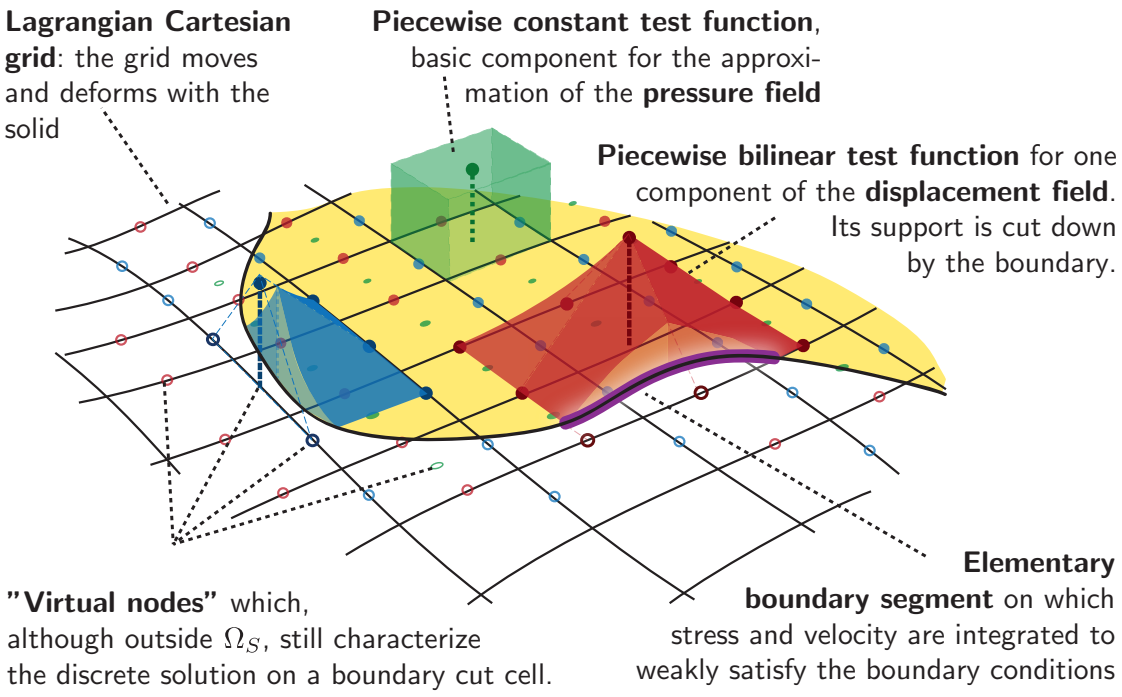

Figure 2.3: *Spatial discretization of the solid structure with a Finite Element Method.*

Displacement field $\underline{\xi}$: The Sobolev space on which the displacement field $\underline{\xi}$ is defined, $\left(H^1(\Omega_0^S)\right)^2$, is approximated with a finite element subspace. Each displacement component is represented by a piecewise bilinear scalar function defined on a staggered Cartesian grid.

For $i \in \{x, y\}$ and $I \in [\![1, n^S]\!]$, we define the function $\underline{N}_{Ii}^{\xi}(\underline{X}) = N_{Ii}^{\xi}(\underline{X})\ \underline{e}_i$. The unit-piecewise bilinear interpolating functions $N_{Ii}^{\xi}(\underline{X})$ is equal to zero on every nodes of the staggered i-grid other than I, on which it takes the value 1. Values Ii for which the support of $N_{Ii}^{\xi}(\underline{X})$ lies totally outside of Ω_0^S are not useful so not considered. However, some nodes Ii may lie outside the solid computational domain, while their corresponding functions $N_{Ii}^{\xi}(\underline{X})$ may have part of their support inside Ω_0^S. Those nodes are called "virtual nodes" and have to be taken in account. As represented in Figure 2.3, although outside the solid, these virtual nodes still characterize the discrete solution on the cut-cells close to the solid boundary. They can be seen as an extrapolation of $\underline{\xi} \cdot \underline{e}_i$ in the vicinity of the solid.

The computed displacement field is a linear combination of the $\underline{N}^{\xi}_{Ii}$ functions:

$$\underline{\xi}(\underline{X},t) = \sum_{i\in\{x,y\}} \sum_{Ii} \xi_{Ii}(t)\ \underline{N}^{\xi}_{Ii}(\underline{X}) \tag{2.34}$$

$$= \sum_{Ix} \xi_{Ix}(t)\ N^{\xi}_{Ix}(\underline{X})\ \underline{e}_x\ +\ \sum_{Iy} \xi_{Iy}(t)\ N^{\xi}_{Iy}(\underline{X})\ \underline{e}_y \tag{2.35}$$

Hence, linear coefficients $\xi_{Ii}(t)$ are the values $\underline{\xi}(\underline{X}_{Ii},t)\cdot\underline{e}_i$ of the i-component of the displacement at time t for the material point initially at the location $\underline{X}_{Ii}$.

The same space of function is used to approximate the field of body forces $\underline{b}^S_0$ and the imposed Dirichlet velocity $\dot{\underline{\xi}}_D$.

Pressure field p^S: The square-integrable function space $L^2(\Omega^S_0)$ on which is defined the pressure field p^S is approximated by the subspace of piecewise constant functions.

For $I \in [\![1, n^S]\!]$, the unit-piecewise constant functions $N^p_I(\underline{X})$ is equal to zero everywhere but on the cell I, on which it takes the value 1. Values I for which the cell I lies totally outside of Ω^S_0 are not useful so not considered.

The computed pressure field is a linear combination of the N^p_I functions:

$$p^S(\underline{X},t) = \sum_I p^S_I(t)\ N^p_{Ii}(\underline{X}) \tag{2.36}$$

Hence, linear coefficients $p^S_I(t)$ are the values of p^S at time t at the material point initially located at the middle of the cell I.

Stress distribution $\underline{\tau}^S_{D0}$ and $\underline{\tau}$: The square-integrable function spaces $\left(L^2(\Gamma^S_{0v})\right)^2$ and $\left(L^2(\Gamma^{FSI})\right)^2$, on which the Dirichlet boundary and the fluid-structure interface stresses $\underline{\tau}^S_{D0}$ and $\underline{\tau}$ are defined, are approximated by a subspace of piecewise constant functions. Each stress component is piecewise constant on the corresponding staggered grid.

For $i \in \{x,y\}$ and $I \in [\![1, n^S]\!]$, we define the function $\underline{N}^{\tau}_{Ii}(\underline{X}) = N^{\tau}_{Ii}(\underline{X})\ \underline{e}_i$. The unit-piecewise constant functions $N^{\tau}_{Ii}(\underline{X})$ is equal to zero except on the part of the fluid-structure

boundary Γ^{FSI} contained within the staggered i-grid cell I. The function is equal to 1 on this line. Values Ii for which Γ^{FSI} does not run across the cell Ii are not considered.

The computed stress is a linear combination of the $\underline{N}^{\tau}_{Ii}$ functions:

$$\underline{\tau}(\underline{X},t) = \sum_{i\in\{x,y\}} \sum_{Ii} \tau_{Ii}(t)\ \underline{N}^{\tau}_{Ii}(\underline{X}) \tag{2.37}$$

$$= \sum_{Ix} \tau_{Ix}(t)\ N^{\tau}_{Ix}(\underline{X})\ \underline{e}_x\ +\ \sum_{Iy} \tau_{Iy}(t)\ N^{\tau}_{Iy}(\underline{X})\ \underline{e}_y \tag{2.38}$$

Two similar spaces of function are used to approximate the stresses $\underline{\tau}^S_{D0}$ and $\underline{\tau}^S_{N0}$ on the essential boundary Γ^S_{0v} and on the natural boundary $\Gamma^S_{0\tau}$ respectively.

$$\underline{\tau}^S_{D0}(\underline{X},t) = \sum_{i\in\{x,y\}} \sum_{Ii} \tau^{D0}_{Ii}(t)\ \underline{N}^{\tau_{D0}}_{Ii}(\underline{X}) \tag{2.39}$$

$$\underline{\tau}^S_{N0}(\underline{X},t) = \sum_{i\in\{x,y\}} \sum_{Ii} \tau^{N0}_{Ii}(t)\ \underline{N}^{\tau_{N0}}_{Ii}(\underline{X}) \tag{2.40}$$

2.2.3 Ordinary differential system of equation

Using the discretization developed in the previous subsection, the weak formulation (2.27)-(2.30) becomes:

$$\begin{bmatrix} \mathcal{M}^S & & & \\ & 0 & & \\ & & 0 & \\ & & & 0 \end{bmatrix} \begin{bmatrix} \ddot{\xi} \\ 0 \\ 0 \\ 0 \end{bmatrix} + \begin{bmatrix} 0 & & \mathcal{D}^S & \mathcal{T}^S \\ {}^t\mathcal{P}^S & \mathcal{M}^P & & \\ {}^t\mathcal{D}^S & & 0 & \\ {}^t\mathcal{T}^S & & & 0 \end{bmatrix} \begin{bmatrix} \dot{\xi} \\ \dot{p}^S \\ \tau^S_{D0} \\ \tau \end{bmatrix}$$

$$+ \begin{bmatrix} \mathcal{K}^S & \mathcal{P}^S & & \\ & 0 & & \\ & & 0 & \\ & & & 0 \end{bmatrix} \begin{bmatrix} \xi \\ p^S \\ 0 \\ 0 \end{bmatrix} = \begin{bmatrix} \mathcal{M}^S b^S_0 + \mathcal{N}^S \tau^S_{N0} \\ 0 \\ {}^t\mathcal{D}^S\ \dot{\xi}^S_D \\ -\ \mathcal{U}^F \end{bmatrix} \tag{2.41}$$

where the above-mentioned matrices are defined by:

$$\mathcal{M}^S_{Ii,Jj} = \iint_{\Omega^S_0} \underline{N}^\xi_{Ii}(\underline{X}) \cdot \underline{N}^\xi_{Jj}(\underline{X}) \quad d\Omega_0 \tag{2.42}$$

$$\mathcal{K}^S_{Ii,Jj} = 2\mu^S \iint_{\Omega^S_0} \nabla^s \underline{N}^\xi_{Ii}(\underline{X}) : \nabla^s \underline{N}^\xi_{Jj}(\underline{X}) \quad d\Omega_0 \tag{2.43}$$

$$\mathcal{M}^P_{I,J} = -\frac{1}{\lambda^S} \iint_{\Omega^S_0} N^p_I(\underline{X}) \cdot N^p_J(\underline{X}) \quad d\Omega_0 \tag{2.44}$$

$$\mathcal{P}^S_{Ii,J} = - \iint_{\Omega^S_0} \left(\nabla \cdot \underline{N}^\xi_{Ii}(\underline{X})\right) N^p_J(\underline{X}) \quad d\Omega_0 \tag{2.45}$$

$$\mathcal{D}^S_{Ii,Jj} = - \int_{\Gamma^S_{0v}} \underline{N}^\xi_{Ii}(\underline{X}) \cdot \underline{N}^{\tau_{D0}}_{Jj}(\underline{X}) \quad d\Gamma_0 \tag{2.46}$$

$$\mathcal{N}^S_{IiJj} = \int_{\Gamma^S_{0\tau}} \underline{N}^\xi_{Ii}(\underline{X}) \cdot \underline{N}^{\tau_{N0}}_{Jj}(\underline{X}) \quad d\Gamma_0 \tag{2.47}$$

$$\begin{aligned} \mathcal{T}^S_{Ii,Jj}(t) &= - \int_{\Gamma^{FSI}(t)} \underline{N}^\xi_{Ii}\left(\underline{X}(\underline{x})\right) \cdot \underline{N}^\tau_{Jj}\left(\underline{X}(\underline{x})\right) \quad d\Gamma \\ &= - \int_{\Gamma^{FSI}_0} \underline{N}^\xi_{Ii}(\underline{X}) \cdot \underline{N}^\tau_{Jj}(\underline{X}) \left(\frac{d\Gamma(t)}{d\Gamma_0}\right) d\Gamma_0 \end{aligned} \tag{2.48}$$

$$\mathcal{U}^F_{Ii}(t) = \int_{\Gamma^{FSI}(t)} \underline{u}(\underline{x},t) \cdot \underline{N}^\tau_{Ii}\left(\underline{X}(\underline{x})\right) \quad d\Gamma \tag{2.49}$$

Note that, except for $\mathcal{T}^S$ and $\mathcal{U}^F$, previous matrices are expressed in terms of integrals on the reference state of functions defined on this same reference state. Hence, they are not related to the current displacement of the structure, and thus can be computed only once at the beginning of the algorithm.

However, $\mathcal{T}^S$ relies on the integral over the current fluid-structure interface location $\Gamma^{FSI}(t)$ of reference state-related functions. Hence, this matrix depends on the current displacement field $\underline{\xi}(t)$ and has to be computed at each time step.

The calculation for $\mathcal{U}^F$ is developed in the section 2.3 dealing with the fluid modeling.

Whatever the time-discretization chosen, $\underline{\xi}$ and $\underline{\dot{\xi}}$ will be linearly related. Though, our linear discretized system can be seen as symmetric.

Practical details for the computation of those matrices, especially concerning the treatment of cut-cells, are given in Zhu *et al.* [ZWH12]. The exact same procedure as been use for the computation of all our matrices.

2.3 Fluid immersed boundary finite-volume method

On a Cartesian MAC-staggered grid peculiar to the fluid (see Figure 2.2), a new finite-volume immersed boundary method for incompressible flow has been developed by Taira and Colonius [TC07, CT08].

While the solid boundaries are moving, the fluid treatment can be view as Eulerian-Lagrangian. The Eulerian form of the fluid governing equations are solved on a stationary staggered grid, whereas, the solid interface is tracked in a Lagrangian fashion, as suggested by the finite-element method described in the previous section 2.2.

Immersed boundary methods with sharp-interface approach succeed to convey the fluid behavior at the very boundary of the solid [MI05], but are difficult to incorporate to the general fluid equations. On the contrary, in the diffuse-interface method of [TC07], the solid boundary acts on the fluid by a continuous forcing approach: the boundary stress is added to the incompressible Navier-Stokes equation through the introduction of an extra regularization term. Moreover, the no-slip condition is enforced by interpolating the fluid velocity on the fluid-structure boundary. This additional constraint acts like a Lagrange multiplier on fluid equations. Hence, unlike sharp-interface methods for which the spatial discretization scheme depends on the boundary location and must be re-computed at each time-step, with this approach, the general finite-volume scheme remains unchanged and the solving procedure only needs to update the regularization and interpolation operators. Although it does not capture exactly the fluid behavior at the interface (within few grid cells), this approach allows a fast treatment of moving boundaries.

We can re-write the governing equations for the fluid (2.16, 2.18, 2.20, 2.22, 2.24, 2.26), taking advantage of the use of the Dirac delta function $\delta(\underline{x})$ to incorporate the natural boundary conditions within the momentum equation:

$$\begin{aligned}
\partial_t \underline{u} \; - \; \frac{1}{Re}\nabla^2 \underline{u} \; + \; \nabla p^F & \qquad \forall \underline{x} \in \Omega^F \\
+ \; \rho_0^S \int\limits_{\underline{s}\in\Gamma^{FSI}} \underline{\tau}(\underline{s}) \; \delta(\underline{s}-\underline{x}) \; d\Gamma & \\
- \int\limits_{\underline{s}\in\Gamma_v^F} \underline{\tau}_D^F(\underline{s}) \; \delta(\underline{s}-\underline{x}) \; d\Gamma \; &= \; \underline{b}^F - (\underline{u}\cdot\nabla)\underline{u} \\
&\quad + \int\limits_{\underline{s}\in\Gamma_\tau^F} \underline{\tau}_N^F(\underline{s}) \; \delta(\underline{s}-\underline{x}) \; d\Gamma
\end{aligned} \tag{2.50}$$

$$\nabla \cdot \underline{u}(\underline{x}) \; = \; 0 \qquad \forall \underline{x} \in \Omega^F \tag{2.51}$$

$$\iint\limits_{\underline{x}\in\Omega^F} \underline{u}(\underline{x}) \; \delta(\underline{s}-\underline{x}) \; d\Omega \; = \; \underline{u}_D(\underline{s}) \qquad \forall \underline{s} \in \Gamma_v^F \tag{2.52}$$

$$\iint\limits_{\underline{x}\in\Omega^F} \underline{u}(\underline{x}) \; \delta(\underline{s}-\underline{x}) \; d\Omega \; = \; \dot{\underline{\xi}}(\underline{s}) \qquad \forall \underline{s} \in \Gamma^{FSI} \tag{2.53}$$

Usual immersed boundary methods introduce a set of Lagrangian points to represent the surface of the immersed structure and applied appropriate constraints to enforce no-slip along those points [Pes72, MI05]. In our method, in order to combine in a coherent way the structure finite-element approach and the fluid method, discrete Lagrangian points are replaced by Lagrangian test functions.

The fluid-structure interface stress $\underline{\tau}$ has already been discretized using piecewise constant stest functions $N_{Ii}^\tau(\underline{X})$ in (2.37). Apply this linear decomposition on the fluid-structure stress term in (2.50) to obtain:

$$\int\limits_{\underline{s}\in\Gamma^{FSI}(t)} \underline{\tau}(\underline{s},t) \; \delta(\underline{s}-\underline{x}) \; d\Gamma = \sum_{i\in\{x,y\}} \sum_{Ii} \tau_{Ii}(t) \left[\int\limits_{\underline{s}\in\Gamma^{FSI}(t)} \underline{N}_{Ii}^\tau\left(\underline{X}(\underline{s})\right) \; \delta(\underline{s}-\underline{x}) \; d\Gamma \right] \tag{2.54}$$

To couple the structure and the fluid systems of equation, the no-slip condition (2.53) should be expressed coherently with the formulation obtain on the solid side (2.30). Similarly to what has been done in the previous section, we multiply the no-slip equation (2.53) by any of the shape functions $\underline{N}^{\tau}_{Ii}$ (define in subsection 2.2.2) and integrate over the boundary surface. We end up recovering the previously introduced vector $\mathcal{U}^{F}_{Ii}$ (cf. formula (2.49)).

$$\mathcal{U}^{F}_{Ii}(t) = \iint\limits_{\underline{x}\in\Omega^{F}} \underline{u}(\underline{x},t)\cdot\left[\int\limits_{\underline{s}\in\Gamma^{FSI}(t)} \delta(\underline{x}-\underline{s})\ \ \underline{N}^{\tau}_{Ii}\Big(\underline{X}(\underline{s})\Big)\ d\Gamma\right] d\Omega \tag{2.55}$$

At this point, the fluid-structure interaction stress $\underline{\tau}$ has been discretized following the method previously used on the solid side, and the no-slip condition has been expressed in its weak form, using the same test functions as what has been done for the structure.

We now have to spatially discretize the fluid variables $\underline{u}$ and p^{F}.

Further investigations needed: **The way** (2.50) **has been obtained by incorporating the boundary stress $\underline{\tau}$ as a body force into the Navier-Stokes equation may need some further study. Indeed, although this method is widely used for enforcing the no-slip condition on body with prescribed motion or on structure in rigid-body motion, the computed Lagrange multiplier $\underline{\tau}$ does not correspond any more to the actual boundary stress defined by** (2.24) **but much more to the stress jump across the boundary between the actual and the fictitious flows.**
Using this wrong formulation, the coupling is not valid anymore. We are equating, on both sides of the interface, the velocity (no-slip condition) and two inconsistent stress terms: one is the actual stress (on the solid side), but the other one is not physically relevant.
As will be established in the results section, chapter 3, this problem will need to be address before being able to get any FSI results.

2.3.1 Spatial discretization

A standard finite-volume discretization is used for the fluid [TC07, CT08]. The following explains the two key parts of the method. We first detail the finite-volume discretization process. Then, we explain the choice for the treatment of the Dirac delta function δ.

Finite-volume method. The above system is discretized using a standard staggered Cartezian grid finite-volume method. Note that the fluid Cartezian grid does not necessarily coincide with the grid defined for the structure in 2.2.2. The dimensions of the fluid-related grid are $n^F = n_x^F \times n_y^F$ and h_F is the discrete spacing between points of the square grid. The locations of the variables on the mesh are similar to the one depicted for the structure in figure 2.2.

The fluid computational domain is not only restricted to fluid region Ω^F since a fictitious flow is also computed within the solid region $\Omega^F_{fictitious} = \Omega^S$. Although the virtual flow does not have any useful physical meaning, it represents a computational asset: the Navier-Stokes equation remains discretized on the whole domain, independently of the current boundary location. Hence, matrices and solving methods are left unchanged time-step after time-step. The fluid-structure boundary condition alone need to be re-adapted to enforce the flow at the boundary of the solid. We thus simultaneously compute two flows: the actual flow, which satisfies both the Navier-Stokes equation on the fluid domain Ω^F and the relevant boundary conditions on its boundaries Γ^F_τ, Γ^F_v and Γ^{FSI}; and the fictitious flow, insignificant result of the Navier-Stokes equation applied on the structure domain Ω^S and subject to the no-slip condition on Γ^{FSI}. Note that, if necessary, the Navier-Stokes equation can be distorted in the virtual fluid domain, without affecting the validity of the real flow solution (as long as the equation in Ω^F and the boundary conditions on Γ^{FSI} remains unchanged). This property will be used later, in section 2.3.3, to compensate for the compressibility of the structure.

In a similar fashion as for the solid, variables locations are ordered and are equivalently denote by their position (i, j) or by their ordered index I.

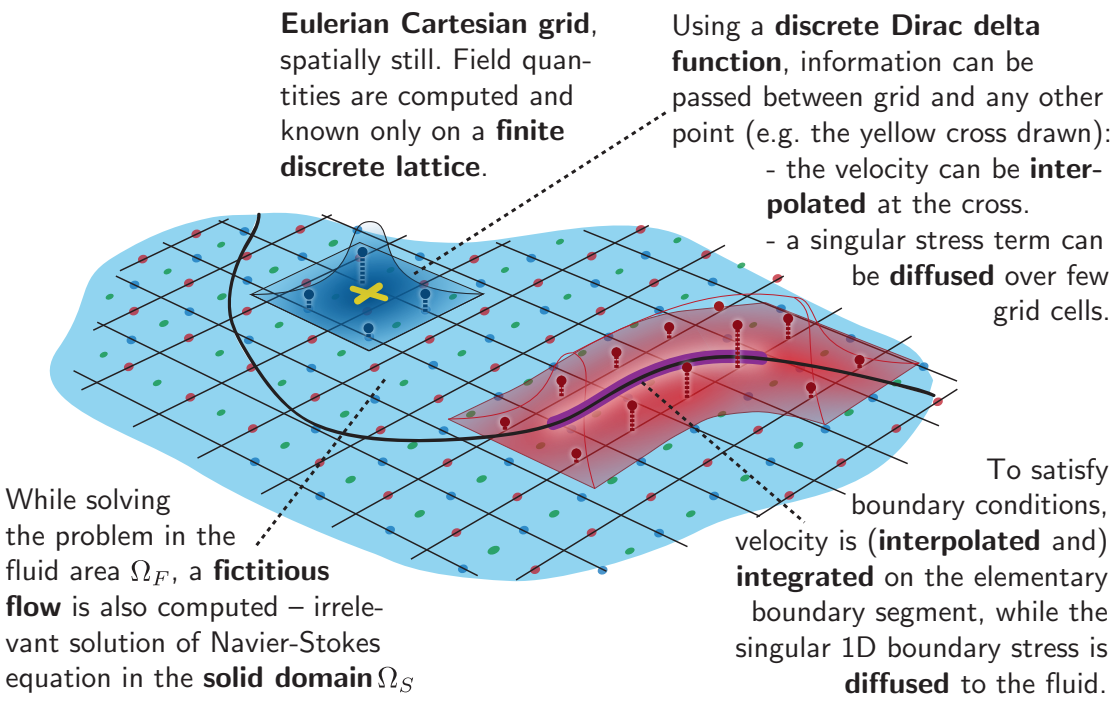

Figure 2.4: *Spatial discretization of the fluid domain with a Finite Volume Method.*

Following the method by Taira & Colonius [TC07], define the velocity flux $\underline{q}$:

$$\underline{q} = h_F \; \underline{u} \tag{2.56}$$

We define differential operators as follows, using the standard finite-volume scheme.

$$h_F \; \nabla \; p^F \left(\underline{x}_{(i,j),p}\right) \quad \longrightarrow \quad (\mathcal{G}p^F)_{(i,j)} = \begin{bmatrix} p^F_{(i,j)} - p^F_{(i-1,j)} \\ p^F_{(i,j)} - p^F_{(i,j-1)} \end{bmatrix} \tag{2.57}$$

$$h_F \; \nabla \cdot \underline{q} \left(\underline{x}_{(i,j),p}\right) \quad \longrightarrow \quad ({}^t\mathcal{G}q)_{(i,j)} = q_{(i+1,j),x} - q_{(i,j),x} + q_{(i,j+1),y} - q_{(i,j),y} \tag{2.58}$$

$$h_F^2 \; \nabla^2 q_k \left(\underline{x}_{(i,j),k}\right) \quad \longrightarrow \quad (\mathcal{L}q_k)_{(i,j)} = q_{(i+1,j),k} + q_{(i-1,j),k} + q_{(i,j+1),k} + q_{(i,j-1),k} - 4q_{(i+1,j),k} \tag{2.59}$$

$$\left.\begin{matrix} h_F(\nabla\times\gamma)_x \left(\underline{x}_{(i,j),x}\right) \\ h_F(\nabla\times\gamma)_y \left(\underline{x}_{(i,j),y}\right) \end{matrix}\right\} \quad \longrightarrow \quad (\mathcal{C}\gamma)_{(i,j)} = \begin{bmatrix} \gamma_{(i,j+1)} - \gamma_{(i,j)} \\ -\left(\gamma_{(i+1,j)} - \gamma_{(i,j)}\right) \end{bmatrix} \tag{2.60}$$

$$h_F \; \nabla \times \underline{q} \; \left(\underline{x}_{(i,j),\gamma}\right) \quad \longrightarrow \quad ({}^t\mathcal{C}q)_{(i,j)} = q_{(i,j),y} - q_{(i-1,j),y} - (q_{(i,j),x} - q_{(i,j-1),x}) \tag{2.61}$$

Note that the curl operator $\mathcal{C}$ is constructed such that its columns are a basis of the

null-space of the divergence operator ${}^t\mathcal{G}$:

$$ {}^t\mathcal{G}\mathcal{C} = 0 \qquad\qquad {}^t\mathcal{C}\mathcal{G} = 0 \tag{2.62} $$

This property is going to be the foundation of the null-space approach explained further below.

Discrete delta function. Before being able to fully discretize the fluid governing equations (2.50)-(2.53), we have to discretize the remaining terms: the fluid velocity on the boundary $\mathcal{U}^F$ expressed in (2.55) and the fluid-structure interaction stress (2.54).

Both of those terms involve the Dirac delta function $\delta(\underline{x} - \underline{s})$ with $\underline{x} \in \Omega^F$ and $\underline{s} \in \Gamma^{FSI}$. After the finite-volume discretization, the discrete fluid points do not span continuously the Lagrange boundary location. We need to express a discrete version δ_{h_F} of the Dirac delta function which connects the Lagrangian boundary location to the Eulerian grid space.

Among the large variety of used discrete delta functions, we use the one developed by Roma *et al.* [RPB99]. Designed for staggered grids, it has the computational advantage of being supported by a small number of cells.

In our 2 dimensional model, the continuous delta function δ is approximated as follows:

$$ \delta_{h_F}(\underline{z}) = \frac{1}{h_F^2} \;\; \phi\left(\frac{z_x}{h_F}\right) \;\; \phi\left(\frac{z_y}{h_F}\right) \tag{2.63} $$

$$ \text{where:} \qquad \phi(r) = \begin{cases} \dfrac{1}{3}\left(1 + \sqrt{1 - 3|r|^2}\right) & \text{for} \quad 0 < |r| < 0.5 \\ \dfrac{1}{6}\left(5 - 3|r| - \sqrt{1 - 3(1 - |r|)^2}\right) & \text{for} \quad 0.5 < |r| < 1.5 \\ 0 & \text{otherwise} \end{cases} \tag{2.64} $$

Hence, ϕ is supported on only 3 cells, and thus δ_{h_F} on only 9 nodes.

We can now define the two discrete operators, discretized versions of (2.54) and (2.55), which pass the information from the solid boundary location to the surrounding fluid and vice versa. An interpolation operator $\mathcal{E}$ would interpolate the fluid velocity field from the staggered grid to the solid boundary Lagrangian shape functions. This operator will enforce

the no-slip condition (2.55). A regularization operator $\mathcal{H}$ would diffuse on the neighboring fluid cells the boundary stress developed in (2.54). A schematic representation of those operators are displayed on figure 2.4

The discretization of (2.55) on the staggered-grid gives:

$$\mathcal{U}^F_{Ii}(t) = h_F^2 \sum_{j\in\{x,y\}} \sum_J u_{Jj}\ \delta_{i,j} \left[\int\limits_{\underline{s}\in\Gamma^{FSI}(t)} \delta_{h_F}(\underline{x}_{Jj} - \underline{s})\ \ \underline{N}^\tau_{Ii}\Big(\underline{X}(\underline{s})\Big)\ d\Gamma \right] \tag{2.65}$$

$$= h_F^2 \sum_{j\in\{x,y\}} \sum_J \frac{q_{Jj}}{h_F}\ \delta_{i,j} \left[\int\limits_{\underline{s}_0\in\Gamma_0^{FSI}} \delta_{h_F}\big(\underline{x}_{Jj} - \underline{x}(\underline{s}_0,t)\big)\ \underline{N}^\tau_{Ii}(\underline{s}_0)\ \left(\frac{d\Gamma(t)}{d\Gamma_0}\right)\ d\Gamma_0 \right] \tag{2.66}$$

Define the extrapolation operators $\mathcal{E}(t)$ so that $\mathcal{U}^F = \mathcal{E}\ q$. Note that test function $\underline{N}^\tau_{Ii}$ has been defined in section 2.2.2 as a piece-wise constant function equal to one on its support $C^S_{0_{Ii}}$ (where $C^S_{0_{Ii}}$ is the I^{th} i-staggered cell of the solid mesh in reference state).

$$\mathcal{E}_{Ii,Jj}(t) = \ \delta_{i,j}\ h_F \int\limits_{\underline{s}_0\in\Gamma_0^{FSI}\cap C^S_{0_{Ii}}} \delta_{h_F}\big(\underline{x}_{Jj} - \underline{x}(\underline{s}_0,t)\big)\ \left(\frac{d\Gamma(t)}{d\Gamma_0}\right)\ d\Gamma_0 \tag{2.67}$$

Similarly, define the regularization operator $\mathcal{H}(t)$ so that $\mathcal{H}\,\tau$ can be identified to the fluid-structure interaction stress term expressed in (2.54) (within a factor h_F).

$$\mathcal{H}_{Jj,Ii}(t) = \ \delta_{i,j}\ h_F \int\limits_{\underline{s}_0\in\Gamma_0^{FSI}\cap C^S_{0_{Ii}}} \delta_{h_F}\big(\underline{x}(\underline{s}_0,t) - \underline{x}_{Jj}\big)\ \left(\frac{d\Gamma(t)}{d\Gamma_0}\right)\ d\Gamma_0 \tag{2.68}$$

According to their definitions, those two operators are transposed from one another:

$$\mathcal{H} = \ {}^t\mathcal{E} \tag{2.69}$$

To compute the integral defining $\mathcal{E}$, we use the trapezoidal rule. Each edge segment $\Gamma_0^{FSI}\cap C^S_{0_{Ii}}$ is split in $\bigcup\limits_k [\underline{s}^k_{0_{Ii}}, \underline{s}^{k+1}_{0_{Ii}}]$, where $\underline{s}^k_{Ii} = \underline{x}(\underline{s}^k_{0_{Ii}})$ are the intersection points between the edge segments and the doubly-refined fluid grid.

$$\mathcal{E}_{Ii,Jj}(t) \approx\ \delta_{i,j}\ h_F \sum_k \frac{\delta_{h_F}\big(\underline{x}_{Jj} - \underline{s}^k_{Ii}(t)\big) + \delta_{h_F}\big(\underline{x}_{Jj} - \underline{s}^{k+1}_{Ii}(t)\big)}{2} \|\underline{s}^{k+1}_{Ii}(t) - \underline{s}^k_{Ii}(t)\| \tag{2.70}$$

We are now able to fully discretize our sytem of equations (2.50)-(2.53). Define the constant scalar β as:

$$\beta = \frac{1}{h_F^2 \; Re} \tag{2.71}$$

We obtain the following discretized system.

$$\dot{q} \; - \; \beta \; \mathcal{L} \; q + \mathcal{G} \; p^F \; - \; {}^t\mathcal{E}_D \; \tau_D^F \; + \; \rho_0^S \; {}^t\mathcal{E} \; \tau \; = \; h_F \; b^F - \; \mathcal{N}^F(q) \; + \; {}^t\mathcal{E}_N \; \tau_N^F + bc_1 \tag{2.72}$$

$${}^t\mathcal{G} \; q \; = \; 0 \; - \; bc_2 \tag{2.73}$$

$$\mathcal{E}_D \; q \; = \; \mathcal{E}_D \; (h_F \; u_D) \tag{2.74}$$

$$\mathcal{E} \; q \; = - \; {}^t\mathcal{T}^S \dot{\xi} \tag{2.75}$$

where $\mathcal{E}_D$ and $\mathcal{E}_N$ are two matrices similar to $\mathcal{E}$ in (2.67) but defined on the essential and natural boundaries respectively. Note that they are defined in reference state, so the formula must be changed accordingly. Matrix $\mathcal{T}^S$ has been defined in the previous structure-related section in (2.48). $\mathcal{N}^F$ represents the convective operator, defined by:

$$\mathcal{N}^F(q) = \frac{1}{h^F} \left(\underline{q} \cdot \nabla \right) \underline{q} = h^F \; \left(\underline{u} \cdot \nabla \right) \underline{u} \tag{2.76}$$

Finally, bc_1 and bc_2 are boundary terms arising from the discretization of the differential operator. Each equation with differential operators involves those kinds of boundary corrections. From now on, we do not explicitly write them, but one must keep in mind that a correction should be done to enforce the relevant boundary condition at the border of the computational domain.

This system of equations (2.72)-(2.75) has to be satisfied at any node I lying within the fluid domain Ω^F. For computing efficiency, we want to avoid modifying the involved operators at each time-step. Only $\mathcal{E}$ is intrinsically time dependent because it has to adapt to the interface motion. Other operators are defined regardless of the belonging of the nodes to Ω^F or Ω^S. Hence, by solving this system, we also compute a virtual flow overlapping

the solid. This is the solution obtained by applying Navier-Stokes equation in Ω^S. We will see in section 2.3.3 that the incompressible Navier-Stokes equations may need to be relaxed in the virtual flow domain to consistently satisfy the no-slip boundary condition with the compressible solid.

2.3.2 Fast method vorticity approach

The flow solver strategy is based on the null-space method with fast Fourier transform developed by Colonius & Taira [CT08]. In this method, benefit is taken from the incompressible nature of the flow to drop the pressure contribution. The computed variable is the discrete vorticity, from which one can obtain the desired velocity and pressure field $\underline{u}$ and p^F.

According to the incompressibility constraint (2.73), the solution $\underline{q}$ we are looking for should belong to the null-space of ${}^t\mathcal{G}$. Since the curl operator $\mathcal{C}$ is a basis of this null-space (see (2.62)), we can define s the discrete streamfunction as:

$$q \;=\; \mathcal{C}\; s \tag{2.77}$$

With this definition for q, the incompressibility equation (2.73) is automatically satisfied.

We also defined the local circulation field γ as follows. γ can be thought as the vorticity times the cell area h_F^2.

$$\gamma \;=\; {}^t\mathcal{C}\; q \;=\; {}^t\mathcal{C}\; \mathcal{C}\; s \;=\; -\;\mathcal{L}\; s \tag{2.78}$$

Note that, according to the discrete differential operators definition:

$$\mathcal{L}\; s \;=\; -\;{}^t\mathcal{C}\; \mathcal{C}\; s \qquad\qquad \forall s,\ \text{scalar field} \tag{2.79}$$

$$\mathcal{L}\; q \;=\; -\;\mathcal{C}\; {}^t\mathcal{C}\; q \qquad\qquad \forall q,\ \text{vector field if} \quad \mathcal{D}\; q = 0 \tag{2.80}$$

By left-multiplying the momentum equation (2.72) with ${}^t\mathcal{C}$, we can remove the pressure gradient term, $\mathcal{G}p^F$. Using the definition of the circulation γ, we obtain a new momentum equation:

$$\dot{\gamma} \;-\; \beta\; \mathcal{L} \quad \gamma - {}^t(\mathcal{E}_D\mathcal{C})\; \tau_D^F \;+\; \rho_0^S\; {}^t(\mathcal{E}\mathcal{C})\; \tau \;=\; {}^t\mathcal{C}\; \left(\; h^F\; b^F - \;\mathcal{N}^F(q) \;+\; {}^t\mathcal{E}_N\; \tau_N^F \;\right) \tag{2.81}$$

The discrete Laplacian $\mathcal{L}$ is diagonalized by a sine transform. As in [CT08], denote by S the sine transform operator, normalized to be equal to its own inverse:

$$\hat{\gamma} = S\ \gamma \ \longleftrightarrow\ \gamma = S\ \hat{\gamma} \tag{2.82}$$

Thus, we symbolically denote by Λ the diagonal matrix of eigenvalues of ${}^t\mathcal{C}\mathcal{C} = -\mathcal{L}$. According to the definitions of s and γ, (2.77) and (2.78), q can be recovered from γ within a constant $q_{uniform}$. Boundary conditions have to be used to fix its value.

$$\Lambda = S\ {}^t\mathcal{C}\mathcal{C}\ S = -\ S\ \mathcal{L}\ S \quad \longleftrightarrow \quad \mathcal{L} = -\ {}^t\mathcal{C}\mathcal{C} = -\ S\ \Lambda\ S \tag{2.83}$$

$$q = \mathcal{C}\ S\Lambda^{-1}S\ \gamma\ +\ q_{uniform} \tag{2.84}$$

γ can thus substitute q in the governing equations (2.81),(2.73)-(2.75). This is the computationally interesting advantage of the null-space approach since the number of variables has been dropped significantly: in 2 dimensions, the scalar field γ contains half the number of degree of freedom in the vector field q. We obtain the system of equations related to the fluid, which can be expressed as follows in matrix notation:

$$\begin{bmatrix} \mathbb{I} & & \\ & \cdot & \\ & & \cdot \end{bmatrix} \begin{bmatrix} \dot{\gamma} \\ \cdot \\ \cdot \end{bmatrix} + \begin{bmatrix} \beta S\Lambda S & -\ {}^t(\mathcal{E}_D\mathcal{C}) & \rho_0^S\ {}^t(\mathcal{E}\mathcal{C}) \\ \mathcal{E}_D\mathcal{C}S\Lambda^{-1}S & \cdot & \\ \mathcal{E}\ \mathcal{C}S\Lambda^{-1}S & & \cdot \end{bmatrix} \begin{bmatrix} \gamma \\ \tau_D^F \\ \tau \end{bmatrix} = \begin{bmatrix} {}^t\mathcal{C}\big(\ h^F\ b^F - \mathcal{N}^F(q) + \ {}^t\mathcal{E}_N\tau_N^F\big) \\ h_F\ \ \mathcal{E}_D u_D - \mathcal{E}_D q_{uniform} \\ -\ {}^t\mathcal{T}^S\dot{\xi}\ -\ \mathcal{E}\ q_{uniform} \end{bmatrix} \tag{2.85}$$

We will see in section 2.5 how we can fully take benefit of the sine Fourier transform to efficiently solve this system.

Possible optimization: The use of the Fast Fourier transform to solve the vorticity Poisson equation restrict the choice of boundary conditions to Neumann, Dirichlet or periodic. To limit the effect of the wall on the computation, one needs to use extensively large domain. The use of the multigrid method developed by Colonius and Taira [CT08] appears to be the suitable solution.

2.3.3 Compressibility correction

As it has already been explained at the end of section 2.3.1, the system of equations (2.85) must be satisfied at any nodes I of the fluid domain Ω^F. However, this system is defined on the whole computational domain $\Omega = \Omega^F \cup \Omega^S$. Hence, by solving 2.3.1, we solve both for the wanted flow field and for the irrelevant solution of the incompressible Navier-Stokes equation subject to the same no-slip and stress boundary conditions.

The fluid-structure interface delimits simultaneously two close domains: the compressible structure and the incompressible virtual flow. An obvious contradiction arises when the volume of the compressible structure is brought to change, due to an overall dilatation or shrinkage.

To overcome this issue, the incompressibility equation (2.73) valid in the actual flow domain must be relaxed for the fictitious flow in Ω^S: a source or sink term must be added. This modification does not affect the validity of the equations in Ω^F since incompressibility must still be satisfied in this region. Further details and remarks regarding the way of implementing this correction are given in Appendix A.

2.4 Time discretization

Over the last two sections 2.2 and 2.3, we went through the spatial discretization of our system. Even if different approaches have been used for the solid and for the fluid, care has been taken to couple them rigorously: no-slip condition and boundary stresses have been set coherently with both the structure finite-element and the fluid finite-volume methods.

We can now bring together the coupled systems (2.41) and (A.14) into one ordinary differential matrix equation. To lighten the problem, Dirichlet boundary conditions are dropped in the remaining part of the text. The procedure to solve those boundary constraints can be strongly inspired from the method used to enforce the fluid-structure boundary conditions.

In the obtained ordinary differential equation (2.86) displayed below, the composite unknown vector, whose first and second time-derivatives are also involved, results from the gathering of solid (ξ and p^S), fluid (γ) and interaction (τ) variables. This system attests that the physical coupling has been properly conveyed through the discretized equation.

$$\begin{bmatrix} \mathcal{M}^S & & & \\ & \cdot & & \\ & & \mathbb{I} & \\ & & & \cdot \end{bmatrix} \begin{bmatrix} \ddot{\xi} \\ \cdot \\ \dot{\gamma} \\ \cdot \end{bmatrix} + \begin{bmatrix} \cdot & \cdot & & \mathcal{T}^S \\ {}^t\mathcal{P}^S & \mathcal{M}^P & & \\ & & \beta S\Lambda S & \rho_0^S\, {}^t(\mathcal{EC}) \\ {}^t\mathcal{T}^S & & \mathcal{EC}S\Lambda^{-1}S & \cdot \end{bmatrix} \begin{bmatrix} \dot{\xi} \\ \dot{p}^S \\ \gamma \\ \tau \end{bmatrix}$$
$$+ \begin{bmatrix} \mathcal{K}^S & \mathcal{P}^S & & \\ & \cdot & & \\ & & \cdot & \\ & & & \cdot \end{bmatrix} \begin{bmatrix} \xi \\ p^S \\ \cdot \\ \cdot \end{bmatrix} = \begin{bmatrix} \mathcal{M}^S b_0^S + \mathcal{N}^S \tau_{N0}^S \\ \cdot \\ {}^t\mathcal{C}\big(\, h^F b^F - \mathcal{N}^F(q) + \ {}^t\mathcal{E}_N \tau_N^F\big) \\ -\mathcal{E} q_{uniform} \end{bmatrix} \tag{2.86}$$

One must note that, except for $\mathcal{T}^S$ and $\mathcal{E}$, no matrix involved in (2.86) is time-dependent. Their computation will have to be done once, at the beginning of the algorithm. The two remaining matrices are intrinsically time-dependent since they characterize the current position of the moving fluid-structure boundary.

Possible optimization: **If τ is defined as the boundary stress expressed in the solid reference state coordinates rather than in the current state coordinates, the matrix $\mathcal{T}^S$ would be constant in time and would not need to be computed at each time step. Indeed, the $\left(\frac{d\Gamma(t)}{d\Gamma_0}\right)$ term in both matrices $\mathcal{T}^S$ and $\mathcal{E}$ definitions** (2.48) **and** (2.67) **would be dropped, so that $\|\underline{s}_{Ii}^{k+1}(t) - \underline{s}_{Ii}^{k}(t)\|$ in** (2.70) **would have to be changed into $\|\underline{s}_{0_{Ii}}^{k+1} - \underline{s}_{0_{Ii}}^{k}\|$. Hence, only $\mathcal{E}$ would be time-dependent.**

2.4.1 The Newmark scheme

To discretize in time the previous differential equation, the Newmark scheme has been used. Through two tunable parameters δ and θ, this scheme allows an efficient discretization of 3-stage differential equation.

The Newmark scheme relates, as follows, any time-dependent variable $X(t)$ and its first and second time derivative [All07] . The subscripts n and $n+1$ refer to the approximation of any variable X at time $n\Delta t$ and $(n+1)\Delta t$ respectively.

$$\frac{\dot{X}^{n+1} - \dot{X}^{n}}{\Delta t} = \delta\ \ddot{X}^{n+1} + (1-\delta)\ \ddot{X}^{n} \tag{2.87}$$

$$\frac{\left(\dfrac{X^{n+1} - X^{n}}{\Delta t}\right) - \dot{X}^{n}}{\Delta t/2} = 2\theta\ddot{X}^{n+1} + (1-2\theta)\ddot{X}^{n} \tag{2.88}$$

The parameter $\delta \in [0,1]$ is known to induce the following behaviors in terms of stability, convergence and accuracy [CMP02]:

- $\delta < \dfrac{1}{2}$ leads to an unstable system
- $\delta = \dfrac{1}{2}$ leads to the accurate 2^{nd} order θ-scheme
- $\delta > \dfrac{1}{2}$ leads to a robust, but dissipative, 1^{st} order scheme

Our system does not need the introduction of numerical dissipation, we set the value of δ to $\dfrac{1}{2}$ in order to reach the highest order of accuracy. With this set-up, the parameter $\theta \in [0, 1/2]$ influences the system in the following way:

- $\theta < \dfrac{\delta}{2} = \dfrac{1}{4}$ leads to a conditionally stable system
  - $\theta = 0$ is the explicit scheme
  - $\theta = 1/12$ leads to the 4^{th} order Fox-Goodwin scheme
  - $\theta = 1/6$ leads to the linear-acceleration scheme
- $\theta \geq \dfrac{\delta}{2} = \dfrac{1}{4}$ leads to an unconditionally stable system
  - $\theta = 1/4$ is the constant-average-acceleration or trapezoidal scheme

2.4.2 Current choice of discretization

We discretize in time our system of equation setting the Newmark coefficients δ and γ as follows to obtain an unconditionally stable 2^{nd} order scheme.

$$\delta = \frac{1}{2} \qquad\qquad \beta = \frac{1}{4} \tag{2.89}$$

All the unknowns in the differential equation (2.86), evaluates at time $(n+1)\Delta t$, can be expressed using the previous time-step and the components of the unknown velocity vector at time-step $(n+1)$ $(\dot{\xi}^{n+1}, \dot{p}^{S^{n+1}}, \gamma^{n+1}, \tau^{n+1})$:

$$\xi^{n+1} = \left[\frac{\theta\ (\Delta t)}{\delta}\right] \dot{\xi}^{n+1} + \qquad \left[\xi^n + (\Delta t)\left(1 - \frac{\theta}{\delta}\right)\dot{\xi}^n + \frac{\Delta t^2}{2}\left(1 - 2\frac{\theta}{\delta}\right)\ddot{\xi}^n\right] \tag{2.90}$$

$$\ddot{\xi}^{n+1} = \left[\frac{1}{\delta\ (\Delta t)}\right] \dot{\xi}^{n+1} - \frac{1}{\delta\ (\Delta t)}\left[\dot{\xi}^n + (\Delta t)(1-\delta)\ \ddot{\xi}^n\right] \tag{2.91}$$

$$p^{n+1} = \left[\frac{\theta\ (\Delta t)}{\delta}\right] \dot{p}^{n+1} + \qquad \left[p^n + (\Delta t)\left(1 - \frac{\theta}{\delta}\right)\dot{p}^n + \frac{\Delta t^2}{2}\left(1 - 2\frac{\theta}{\delta}\right)\ddot{p}^n\right] \tag{2.92}$$

$$\dot{\gamma}^{n+1} = \left[\frac{1}{\delta\ (\Delta t)}\right] \gamma^{n+1} - \frac{1}{\delta\ (\Delta t)}\left[\gamma^n + (\Delta t)\Big(1-\delta\Big)\ \dot{\gamma}^n\right] \tag{2.93}$$

Before obtaining a fully discretized system, we still have to deal with the non-linear advective term $\mathcal{N}^F(q)$ defined by (2.76) and the time-dependent matrices $\mathcal{T}^S(t)$ and $\mathcal{E}(t)$ defined in (2.48) and (2.70).

- The commonly used 2^{nd} order Adams-Bashforth method is applied to express $\mathcal{N}^F(q)$ at time-step $n+1$:

$$\left(\mathcal{N}^F(q)\right)^{n+1} = 2\mathcal{N}^F(q^n) - \mathcal{N}^F(q^{n-1}) \tag{2.94}$$

$$= \frac{2}{h^F}\left(\underline{q}^n \cdot \nabla\right)\underline{q}^n - \frac{1}{h^F}\left(\underline{q}^{n-1} \cdot \nabla\right)\underline{q}^{n-1} \tag{2.95}$$

- An initial guess of the boundary location at time-step $n+1$ is used to approximate $\mathcal{T}^S(t)$ and $\mathcal{E}(t)$ at time-step $n+1$. We assume constant velocity between time-steps n and $n+1$ to obtain our approximation $\tilde{\xi}$ of ξ^{n+1}. An iterative sub-loop can be used to refine this guess. The corresponding approximated matrices are denoted by $\tilde{\mathcal{T}}^S$ and $\tilde{\mathcal{E}}$.

Possible optimization: **The choice of the Adams-Bashforth method has been made following the example of numerous publications. Besides, the constant velocity assumption for the boundary location has been a choice towards simplicity. Best results might be achieved using more efficient methods.**

2.4.3 Time-discretized linear system

Apply the time-discretization scheme mentioned above on the ordinary differential equation (2.86) to get the following coupled system of equation:

$$\begin{bmatrix} \mathbb{M}^S & \mathbb{P}^S & & \mathbb{R}^S \\ {}^t\mathbb{P}^S & \mathbb{M}^P & & \\ & & \mathbb{M}^F & \mathbb{R}^F \\ \mathbb{T}^S & & \mathbb{T}^F & \end{bmatrix} \begin{bmatrix} \dot{\xi}^{n+1} \\ \dot{p}^{Sn+1} \\ \gamma^{n+1} \\ \tau^{n+1} \end{bmatrix} = \begin{bmatrix} \xi\text{-RHS} \\ \cdot \\ \gamma\text{-RHS} \\ \tau\text{-RHS} \end{bmatrix} \tag{2.96}$$

where we have defined:

$$\mathbb{M}^S = \frac{\theta}{\delta}\,(\Delta t)\;\mathcal{K}^S \quad + \quad \frac{1}{\delta\;(\Delta t)}\;\mathcal{M}^S \tag{2.97}$$

$$\mathbb{M}^P = \frac{\theta}{\delta}\,(\Delta t)\;\mathcal{M}^P \tag{2.98}$$

$$\mathbb{P}^S = \frac{\theta}{\delta}\,(\Delta t)\;\mathcal{P}^S \tag{2.99}$$

$$\mathbb{R}^S = \qquad \tilde{\mathcal{T}}^S \tag{2.100}$$

$$\mathbb{T}^S = \qquad {}^t\tilde{\mathcal{T}}^S \quad + \quad \left(\tilde{\mathcal{E}}\mathcal{G}\Phi\right)\mathcal{Q}^S \tag{2.101}$$

$$\mathbb{M}^F = S\Big(\overbrace{\frac{\mathbb{I}}{\delta\;(\Delta t)}\;+\;\beta\Lambda}^{=\mathcal{D},\text{ diagonal}}\Big)S \;=\; S\mathcal{D}S \tag{2.102}$$

$$\mathbb{R}^F = \;\rho_0^S\;{}^t(\tilde{\mathcal{E}}\;\mathcal{C}) \tag{2.103}$$

$$\mathbb{T}^F = \;(\tilde{\mathcal{E}}\;\mathcal{C})\;S\;\Lambda^{-1}S \tag{2.104}$$

$$\begin{aligned}\xi\text{-RHS} = \quad & \mathcal{M}^S\;b_0^{S\,n+1} + \mathcal{N}^S\;\tau_{N0}^{S\;\;n+1} \\ & + \mathcal{M}^S\frac{1}{\delta\;(\Delta t)}\left[\dot{\xi}^n + (\Delta t)(1-\delta)\;\ddot{\xi}^n\right] \\ & - \mathcal{K}^S\left[\xi^n + (\Delta t)\left(1-\frac{\theta}{\delta}\right)\dot{\xi}^n + \frac{\Delta t^2}{2}\left(1-2\frac{\theta}{\delta}\right)\ddot{\xi}^n\right] \\ & - \mathcal{P}^S\left[p^n + (\Delta t)\left(1-\frac{\theta}{\delta}\right)\dot{p}^n + \frac{\Delta t^2}{2}\left(1-2\frac{\theta}{\delta}\right)\ddot{p}^n\right]\end{aligned} \tag{2.105}$$

$$\begin{aligned}\gamma\text{-RHS} = \quad & {}^t\mathcal{C}\left(\;h^F b^{F\,n+1} - \;\left(2\mathcal{N}^F(q^n) - \mathcal{N}^F(q^{n-1})\right)\;+\;{}^t\tilde{\mathcal{E}}_N\tau_N^{F\,n+1}\right) \\ & + \frac{1}{\delta\;(\Delta t)}\left[\gamma^n + (\Delta t)(1-\delta)\;\dot{\gamma}^n\right]\end{aligned} \tag{2.106}$$

$$\tau\text{-RHS} = -\;\tilde{\mathcal{E}}\;q_{uniform} \tag{2.107}$$

On this system, one can notice that the first 2×2 block-submatrix constitutes the system one would have obtained with the structure taken alone, without any fluid to interact with.

This matrix is sparse and symmetric, but unfortunately non-positive definite [ZWH12]. The matrix $\mathbb{M}^F$, particularly easy to invert knowing it can be expressed as the discrete sine transpose of a diagonal matrix, would be the matrix resulting from the fluid system taken alone [CT08].

The coupling is expressed through the remaining four submatrices: the interpolation matrices $\mathbb{T}^S$ and $\mathbb{T}^F$ and the regularization matrices $\mathbb{R}^S$ and $\mathbb{R}^F$. The bottom block-row enforces the no-slip condition at time-step $n+1$. The two sub-matrices in the right block-column, on which acts the same unknown τ^{n+1}, enforces the stress balance through the boundary. The stress vector τ^{n+1} can be viewed as a Lagrange multiplier. Its role is similar to the effect the pressure has on the momentum Navier-Stokes equation to satisfy the divergence-free constraint. In this way, the current fluid-structure interaction method removes slip through a projection, by enforcing the proper stress on either side of the boundary.

The boundary force is determined "implicitly" allowing the use of larger CFL numbers compared to some past methods. This enforcement is not properly implicit since no-slip conditions and stress balance are actually enforced at the location the boundary is explicitly guessed to be: matrices $\tilde{\mathcal{T}}^S$ and $\tilde{\mathcal{E}}$ are used instead of $\mathcal{T}^{S^{n+1}}$ and $\mathcal{E}^{n+1}$.

2.5 System solving procedure: Fractional step method

In earlier sections, we have conducted spatial and time discretizations of our coupled problem and reached the coupled linear system of equation (2.96). Its structure properties have been discussed in the previous section. We now present a rather efficient solving procedure, the fractional step method (or projection method), which takes benefits of those features.

Our global equation can be viewed, like any system of the form $\left[\begin{smallmatrix} A & B \\ C & \cdot \end{smallmatrix}\right]\left[\begin{smallmatrix} X \\ \lambda \end{smallmatrix}\right] = \left[\begin{smallmatrix} \alpha \\ \beta \end{smallmatrix}\right]$, as a constrained system. In our particular case, the no-slip condition constitutes the generic constraint $CX = \beta$. According to [Per93], those systems can be solved with the three following steps:

- $A\ X^* = \alpha$ Solution X^* of the non-constrained system (2.108)
- $CA^{-1}B\ \lambda = CX^* - \beta$ Projection step: λ solved to satisfy the constraint (2.109)
- $A(X - X^*) = -B\lambda$ Correction step (2.110)

The first and last steps (2.108) and (2.110) consist, in our particular case, in solving the block diagonal matrix where solid and fluid equations are uncoupled. Efficient solving procedures of those system have been developed in [ZWH12] and [CT08] respectively. For the structure, GMRES or LDL algorithm can be used to solve the sparse symmetric non-positive definite system. For the fluid, the discrete Fourier transform is efficiently used.

The second step (2.109) is more subtle. Using the notation in (2.96), this step becomes:

$$\left(\begin{bmatrix} \mathbb{T}^S & \cdot \end{bmatrix} \begin{bmatrix} \mathbb{M}^S & \mathbb{P}^S \\ {}^t\mathbb{P}^S & \mathbb{M}^P \end{bmatrix}^{-1} \begin{bmatrix} \mathbb{R}^S \\ \cdot \end{bmatrix} \quad + \quad \mathbb{T}^F\ (\mathbb{M}^F)^{-1}\ \mathbb{R}^F \right)\ \tau^{n+1} \ = \ \cdots \tag{2.111}$$

The right-hand-side term in the brackets does not raise any particular issue. Indeed, according to its definition (2.102), $\mathbb{M}^F$ inverse is simply $S\mathcal{D}^{-1}S$ where $\mathcal{D}$ is diagonal. However, the left-hand side term is computationally expensive since it involves n_τ solving of a $N_S \times N_S$ linear systems, where n_τ is the (small) number of boundary segments (number of columns in $\mathbb{R}^S$) and N_S is the (big) number of solid unknowns (displacement and pressure). Although all the involved matrices are sparse, the resulting $n_\tau \times n_\tau$ term is dense.

Possible optimization: **A GMRES algorithm is expected to be suitable (in terms of speed and storage) to solve the structure-related equations, both for the step 1,3 and for the step 2 of the fractional step method. A first attempt as been made but was particularly slower than the direct solving with the Matlab LDL-solver for symmetric sparse matrix. This should be improved significantly using an appropriated tuning.**

CHAPTER 3

Application: Vibrating immersed elastic disk

In the previous chapter, the methodology to solve a fluid-structure interaction problem has been explained. We investigate here the performance of the algorithm through its application to a numerical example.

3.1 Problem description

A circular two-dimensional circular elastic structure of radius R_0 is surrounded by an incompressible fluid. Incompressibility is also imposed to the solid for well-posedness. At initial time, the system is perturbed from its equilibrium by prescribed displacement and velocities: $\underline{\xi}(t=0)$, $\dot{\underline{\xi}}(t=0)$ and $\underline{u}(t=0)$.

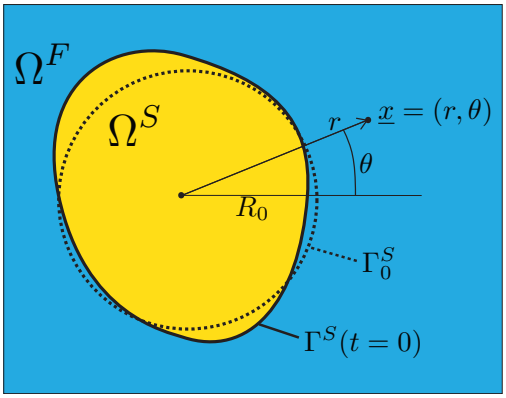

Figure 3.1: *Initially perturbed circular structure surrounded by incompressible fluid.*

3.1.1 Nondimensionalization

According to the nondimensionalization process explained in section 2.1.1, we denote by $L = 2R_0$ the diameter, at equilibrium, of the circular 2D-structure.

Since there is no given characteristic velocity in our system, U_0 is chosen to be the speed of transverse waves in the solid, defined from its density ρ_0^S and its shear modulus μ^S.

$$U_0 = \sqrt{\frac{\mu^S}{\rho_0^S}} \tag{3.1}$$

The two remaining dimensionless parameters are:

$$Re = \frac{\rho^F L U_0}{\mu^F} = \frac{\rho^F L}{\mu^F}\sqrt{\frac{\mu^S}{\rho_0^S}} \qquad\qquad \tilde{\rho}_0^S = \frac{\rho_0^S}{\rho^F} \tag{3.2}$$

The parameter $\tilde{\mu}^S$ in (2.15) has been used to define the reference velocity U_0 so its value is now 1. $\tilde{\lambda}^S$ is not taken in account anymore since its value has to be fixed to infinity to satisfy solid incompressibility. The newly defined "Reynolds number" Re is based on the waves velocity in the solid, due to elasticity, rather than to a characteristic fluid velocity. It characterizes the importance of structure elasticity with regards to fluid viscosity. Although it is not a Reynolds number anymore, the notation Re is kept for consistency with the earlier chapters.

With this dimensionalization in mind, the governing equations of our present problem are the ones in 2.1.2 where μ^S is fixed to 1, no body forces $\underline{b}_0^S$ and $\underline{b}^F$ are applied, and boundaries for the solid are exclusively fluid-structure interfaces Γ^{FSI}, while the fluid domain is also limited by essential boundaries Γ_v^F.

3.1.2 Theoretical solution

Consider the system disturbed from equilibrium by a perturbation small enough (initial condition) so that the advective term in the Navier-Stokes equation (2.18) can be neglected at first order. All remaining terms in the equations governing the fluid-structure coupled system are now linear.

We can solve for the eigenfunctions and obtain the vibrational modes of the system. The algebra has been carried out in Appendix B with the appropriate assumptions.

It has been shown that, for any parameters Re and $\tilde{\rho}_0^S$, a solution of the form:

$$f(r,\theta,t) = \Re\left[\hat{f}(r)e^{i\sigma t}\right] \begin{Bmatrix} \cos(m\theta) \\ \sin(m\theta) \end{Bmatrix} \tag{3.3}$$

may exist to described any variables of the system. The particular values m and σ such that a solution exists are the eigenvalues. σ would be the complex pulsation (its real part is the current pulsation and its imaginary part characterizes the dumping) and m would be the angular mode. $\Re$ stands for the real part operator.

For the case of $m = 2$, one can observe that the free motion of the coupled system is a specific combination (Re and $\tilde{\rho}_0^S$ dependant) of the two vibrational modes of each uncoupled subsystem. Those two distinct sets of modes are as shown in Figure 3.2.

3.1.3 Computed results

At initial time, the fluid-solid system is disturbed along its vibrational mode: all the fields variables are set to be consistent with the oscillatory solution found theoretically.

The solver should then predict the evolution of all solid and fluid quantities, and this evolution should be along the natural vibrational mode.

However, as it has been explained in chapter 2.3 in the **Further investigations needed** paragraph, the boundary stress term on the fluid side has not been inconsistently defined. The FSI solver defined as such is not able to predict the accurate evolution of the coupled system, since the traction balance at the interface is altered.

Since the theoretical solution is known at all time, it is possible to test separately each subsystems by enforcing proper kinematic or dynamic boundary conditions. In this way, all field variables can be solved and the behavior of the two separate subsystems can be further investigated. A reconstructed representation of the results obtained by running separately the solid and the fluid solvers (Figure 3.5) gives a sense of what the coupled FSI code should

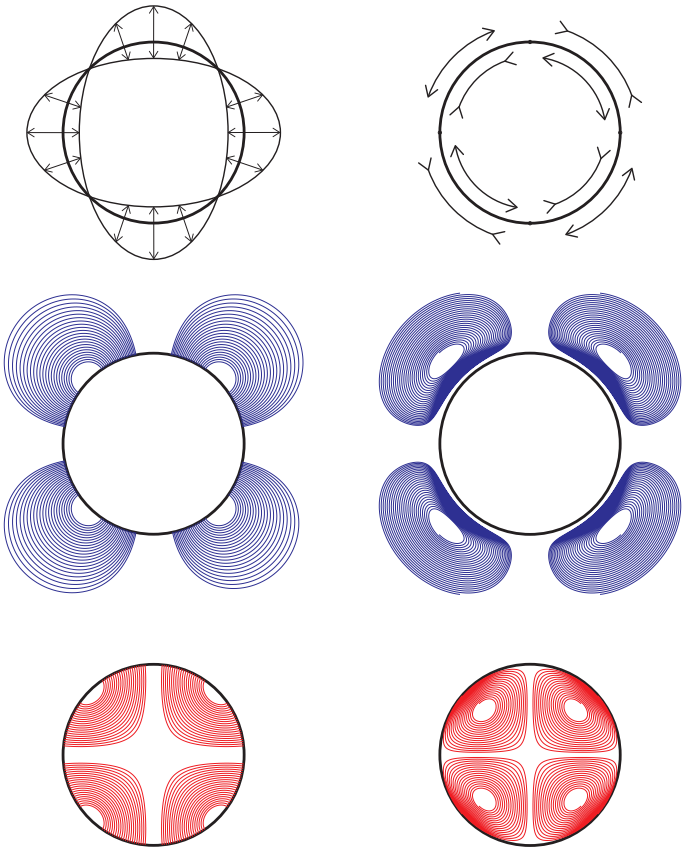

Figure 3.2: *Vibrational modes of uncoupled subsystems. On the top: characteristic motion of the boundary. At the middle: streamlines of the fluid flow field. At the bottom: streamlines of the solid displacement field. On each side: one of the two distinct modes of vibration of the uncoupled subsystems (considered as alone).*

be able to compute. In figure 3.3 are plotted the results of a particular simulation of the fluid solver ($Re = 200$, $\tilde{\rho}_0^S = 10$, $R_0 = 0.5$, $t = \frac{17}{16}T = \frac{17}{16}\frac{2\pi}{\Re[\sigma]}$) with imposed velocity at the boundary, compared to the expected theoretical solution. The two curves are overlaying in the fluid domain. Similarly, on figure 3.4 are displayed the results for the structure code run with imposed traction at the boundary are plotted. The curve representing the solution of the solid test case subject to imposed velocity at the interface is the exact same: in both case, the computed velocity is closed enough to the solution.

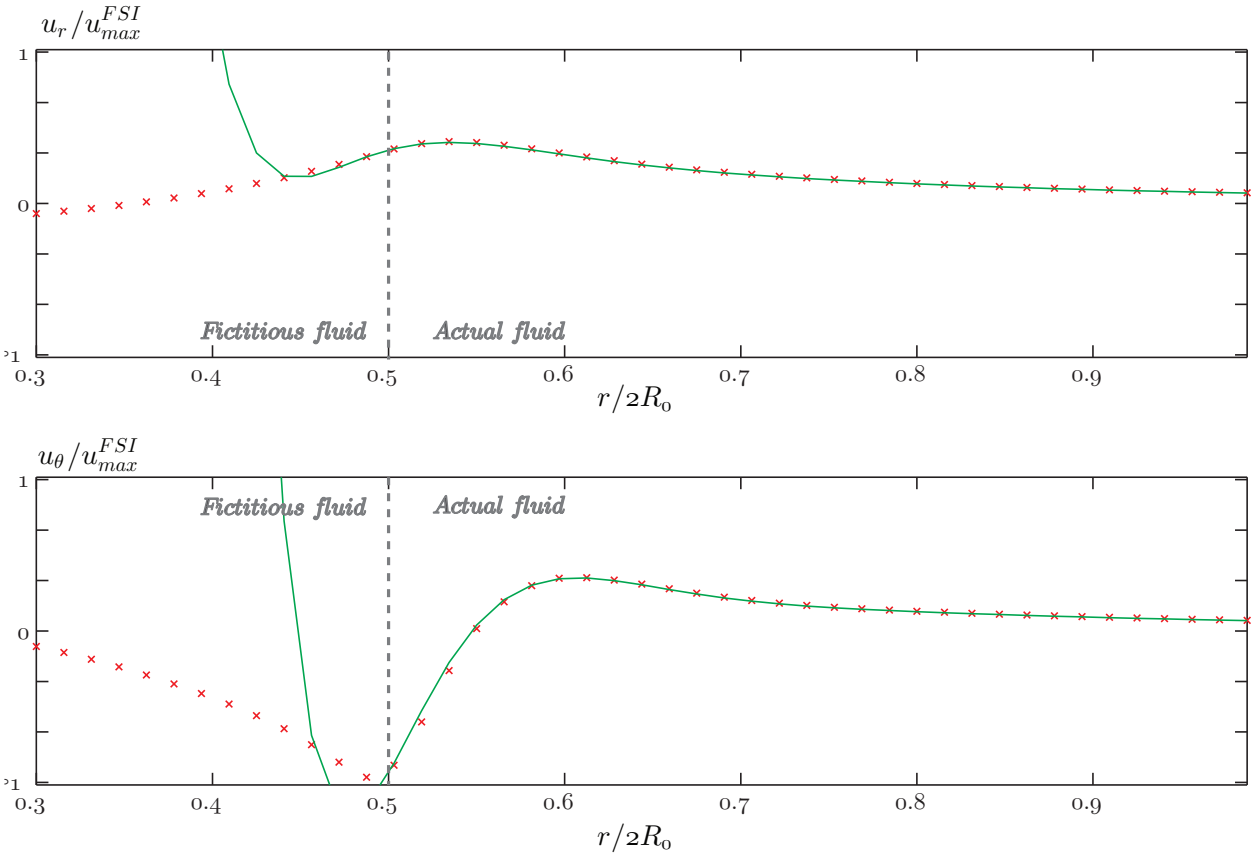

Figure 3.3: *Theoretical and computed fluid velocity profiles (kinematic boundary conditions).* $Re = 200$, $\tilde{\rho}_0^S = 10$, $R_0 = 0.5$, $t = \frac{17}{16}T = \frac{17}{16}\frac{2\pi}{\Re[\sigma]}$. *At the top: radial velocity profile along* $\theta = 0$. *At the bottom: circumferential velocity profile along* $\theta = \pi/2$. *Green solid line: theoretical solution. Red crosses: computed solution*

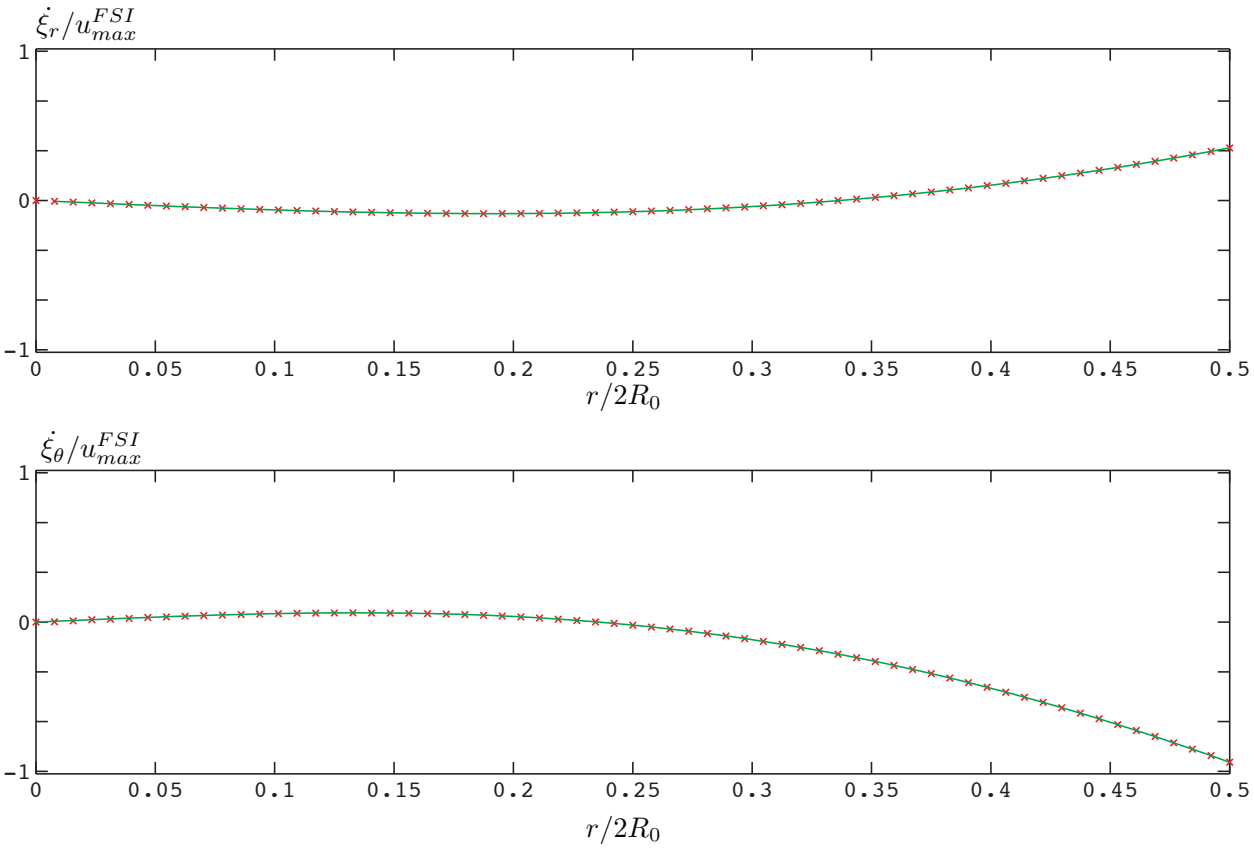

Figure 3.4: *Theoretical and computed solid velocity profiles (dynamic boundary conditions).* $Re = 200$, $\tilde{\rho}_0^S = 10$, $R_0 = 0.5$, $t = \frac{17}{16}T = \frac{17}{16}\frac{2\pi}{\Re[\sigma]}$. *At the top: radial velocity profile along* $\theta = 0$. *At the bottom: circumferential velocity profile along* $\theta = \pi/2$. *Green solid line: theoretical solution. Red crosses: computed solution*

Tables 3.1 and B.1 demonstrate the order of convergence obtained. The wide discrepancy between the different values is not explained, but it can nevertheless be concluded that the code is between first and second order accurate. Results for the properly coupled system should confirm the robustness of the solver to deal with large or small values for the density ratio $\tilde{\rho}_0^S$ and the elasticity-based Reynolds Re.

kinematic/dynamics BCs	$\tilde{\rho}_0^S = 0.1$	$\tilde{\rho}_0^S = 1.0$	$\tilde{\rho}_0^S = 10$
$Re = 40$		1.75 / 1.78	
$Re = 200$	1.71 / 1.90	1.91 / 1.57	1.18 / 1.00
$Re = 1000$		1.34 / 1.09	

Table 3.1: *Order of convergence of the uncoupled solid subsystem (kinematic or dynamic boundary conditions).The rate has been calculated with the 2-norm on simulations of different grid refinements. The first number is the rate of convergence for kinematic boundary conditions (imposed velocity), the second correspond to dynamic conditions (imposed traction)*

kinematic BCs	$\tilde{\rho}_0^S = 0.1$	$\tilde{\rho}_0^S = 1.0$	$\tilde{\rho}_0^S = 10$
$Re = 40$		1.71	
$Re = 200$	2.38	2.11	2.39
$Re = 1000$		2.03	

Table 3.2: *Order of convergence of the uncoupled fluid subsystem (kinematic boundary conditions).The rate has been calculated with the 2-norm on simulations of different grid refinements*

Further investigation needed: We have thus shown the accuracy of our method. The 2^{nd} order convergence rate reached by Zhu *et al.* [ZWH12] has not been conserved through the passage from a static to a dynamic code with weakly enforced IBM. However, the method is still better than first order. Regarding the fluid code, the high rate of convergence (above 2) is quite surprising, and has not been explained. Further study will have to clarify the reason for such results, and consider the global coupled system once the fluid boundary stress issue will have been addressed.

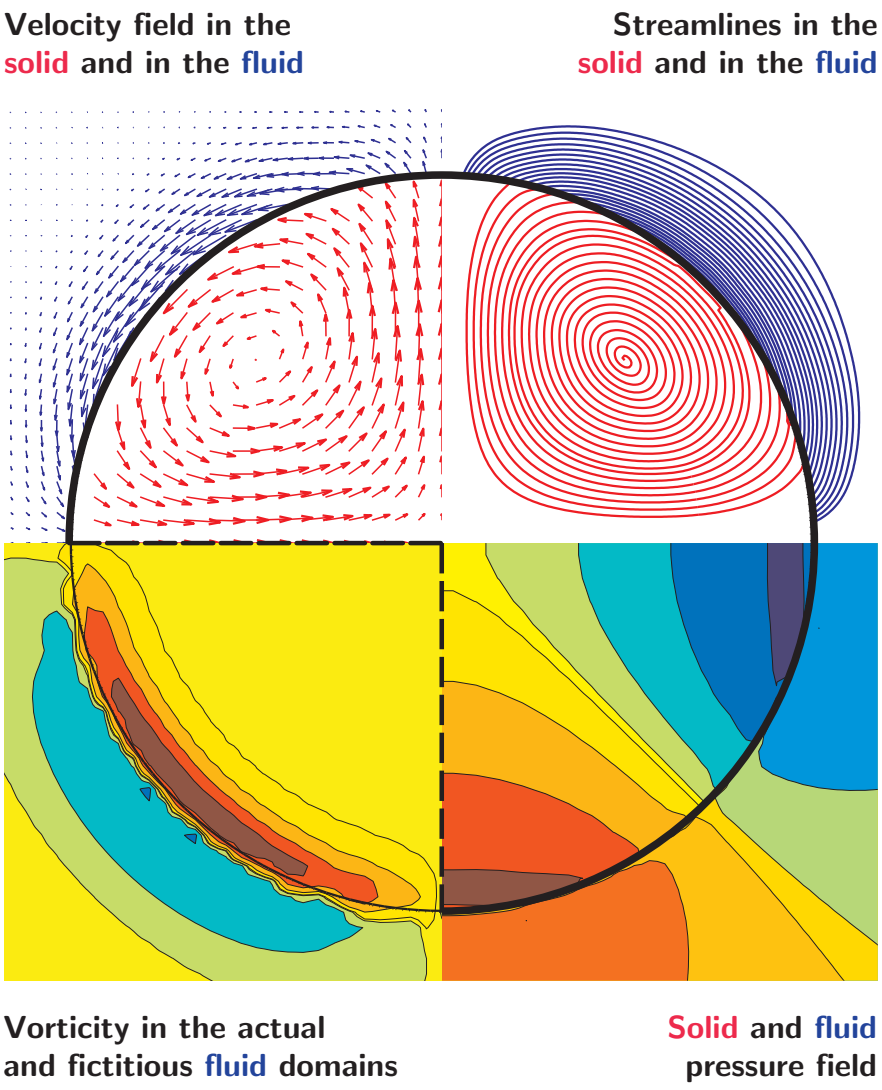

Figure 3.5: *Example of solution fields to be obtained with the current FSI method.* $Re = 40$, $\tilde{\rho}_0^S = 1$

CHAPTER 4

Conclusion

We have described a Fluid-Structure Interaction algorithm which brings together attractive features. Based on Eulerian-Lagrangian framework – Eulerian description of the fluid, Lagrangian treatment of the solid – the technique applies a coherent coupling at the interface of the two systems. The solid code, inspired by the work of Zhu *et al.* [ZWH12], combines a FEM on a uniform Cartesian grid and a corresponding weak-formulation of a sharp IBM. Versatility is gained without sacrificing accuracy [ZWH12]. On the other side, the extremely efficient combination of the null-space approach and the Fast Fourier Transform established by Colonius and Taira [TC07, CT08] has been merged consistently to the solid code. The overall coupled system is then time-discretized and solved as a whole. This should lead to a stable and robust algorithm.

Several implementation works have to be done before reaching the above-mentioned expected algorithm. The main issue remains in the currently inaccurate boundary stress formulation. Slight changes in the system of equation should bring the issue to a close. A proper convergence study will then point out the possible weakness. There is also room for progress in terms of optimization. As mentioned throughout the text, different points can be improved to boost or refine the algorithm.

Future works will head towards the handling of three-dimensional flows, which is going to raise the issue of the solid compressibility. Although the structure has to be incompressible in 2D for well-posedness, the way to account for a volume change in the solid has already been explored. Nevertheless, some questions remain unclear and new ones will certainly be raised!

APPENDIX A

Compressibility correction term

In this appendix are developed the thoughts that have been made regarding the implementation of a corrector to allow the structure to be globally non-divergence-free. Indeed, as it has been explained in section 2.3.3, with the current implementation, we are solving for a fictitious solution of the incompressible Navier-Stokes equations in the solid domains, subject to the no-slip boundary condition. However, if the structure is compressible, its borders do not have any reason to define a volume preserving domain. And this leads to a trivial contradiction.

The solution is to modify the rule governing the fictitious fluid in order to let it tolerate a global dilatation or shrinkage. We thus change the divergence free constraint equation (2.73) into:

$$ {}^t\mathcal{G}q = 0 + h_F^2\ \mathcal{S}^F \qquad\qquad \text{with,} \quad \forall I \in \Omega^F, \quad \mathcal{S}_I^F = 0 \tag{A.1} $$

$\mathcal{S}^F$ is a source (or sink) term whose support lies exclusively into the virtual domain.

The flux field q cannot be written any more as $q = \mathcal{C}s$ like in (2.77), since it does not belong to the null-space of ${}^t\mathcal{G}$. To satisfy the continuity equation, we define a new component q_{irr} of the field q which is not divergence-free in Ω^S (but must be in Ω^F to maintain the incompressibility enforcement of the physical flow). We also impose to this component to be irrotational.

$$ {}^t\mathcal{C}q_{irr} = 0 \tag{A.2} $$

The discrete stream-function s and the local circulation γ, previously defined in (2.77)

and (2.78), must now satisfy the following relations:

$$q = \mathcal{C}s + q_{irr} \tag{A.3}$$

$$\gamma = {}^t\mathcal{C}q = {}^t\mathcal{C}\mathcal{C}s = S\Lambda S\ s \tag{A.4}$$

Note that thanks to (A.2), the definition of γ has not been modified: the vorticity does not feel the presence of this additional irrotational component of the flow. Using those two last equations, we obtain the relation where q is expressed in terms of γ. The constant component $q_{uniform}$ of the vector field, which can be part of both the irrotational and of the potential components of q, is added separately. Boundary conditions for s and for q_{irr} have to be set accordingly.

$$q = \mathcal{C}S\Lambda^{-1}S\ \gamma + q_{irr} + q_{uniform} \tag{A.5}$$

The new system of equations governing the fluid motion is written below.

$$\begin{bmatrix} \mathbb{I} & & \\ & \cdot & \\ & & \cdot \end{bmatrix} \begin{bmatrix} \dot{\gamma} \\ \cdot \\ \cdot \end{bmatrix} + \begin{bmatrix} \beta S\Lambda S & -{}^t(\mathcal{E}_D\mathcal{C}) & \rho_0^S\ {}^t(\mathcal{E}\mathcal{C}) \\ \mathcal{E}_D\mathcal{C}S\Lambda^{-1}S & \cdot & \\ \mathcal{E}\ \mathcal{C}S\Lambda^{-1}S & & \cdot \end{bmatrix} \begin{bmatrix} \gamma \\ \tau_D^F \\ \tau\cdots \end{bmatrix} = \begin{bmatrix} {}^t\mathcal{C}\big(h^F\ b^F - \mathcal{N}^F(q) + {}^t\mathcal{E}_N\tau_N^F\big) \\ \mathcal{E}_D\left(h_F u_D - q_{irr} - q_{unif}\right) \\ -{}^t\mathcal{T}^S\dot{\xi} - \mathcal{E}\left(q_{irr} + q_{unif}\right) \end{bmatrix} \tag{A.6}$$

q_{irr} is irrotational, and so it can be written as the gradient of a scalar potential ϕ (using null-space properties in (2.62)). Since q_{irr} must also satisfy the continuity equation (A.1), ϕ is solution of Poisson's equation:

$$q_{irr} = \mathcal{G}\phi \qquad \text{with} \quad \mathcal{L}\phi = h_F^2\ \mathcal{S}^F \tag{A.7}$$

Boundary conditions: The Poisson's equation (A.7) need the prescription of boundary conditions to be solved.

A problem involving a dilating structure in an incompressible flow must be a 3-dimensional AND infinite problem to be well-posed. Thus, imposing the potential ϕ to be zero at the border of the domain is not physically relevant, even for the domain is large.

We decide to solve the equation (A.7) subject to Neumann boundary condition at infinity. The discrete solution can be computed using a lattice Green's function (discrete version of the usual continuous Green's function). Denote g the lattice Green's function, unique solution (up to a constant) of the equation:

$$\mathcal{L}g = \delta_{(i,j),(0,0)} \tag{A.8}$$

Denote $*$ the convolution product. Then the solution ϕ of the Laplace equation (A.7) is given by:

$$\phi_I = h_F^2 \ \left[g * \mathcal{S}^F\right]_I = h_F^2 \ \sum_J g_{I-J} \ \mathcal{S}_J^F \tag{A.9}$$

Position and distribution of the source S_I^F: Some computational tests exhibit that the source distribution within the fictitious flow domains does not impact the actual flow solution. Only the global flux does. It seems that any change of source location can be accounted for by a distribution of vorticity *inside* the solid domain. This statement needs to be mathematically confirmed.

Thus, we decide to place the source at the center $\underline{x} = \underline{x}\,(\underline{X}_{center}, t)$ of the structure domain. We use the discrete delta function δ_{h_F} defined in (2.63) to regularize, to smear, the source term on the fluid grid. Hence, $\mathcal{S}^F$ is equal to zero everywhere but on the currently neighboring nodes of the solid center. If the volume flow rate is denoted S_0, then:

$$\mathcal{S}_{(i,j)}^F = S_0 \ \ \delta_{h_F}\Big(\underline{x}\,(\underline{X}_{center}, t) - \underline{x}_{(i,j),p}\Big) \tag{A.10}$$

Strenght S_0 of the source term: The volume flow rate S_0 must be maintain such that the pressure of the incompressible fluid decays toward zero at infinity. However, the pressure is not yet accessible at the stage of the calculation S_0 needs to be determined. A solution will have to be found to implicitly constrain p at infinity through the use of the Lagrange multiplier-like coefficient S_0.

Corrector for 2D flow: In 2D, as mentioned earlier, problem with compressible solid are ill-posed. Moreover, when considering the solid as incompressible within the small deformation hypothesis (cf. section 2.1), the enforced continuity equation is $\nabla_0 \cdot \underline{\xi} = \dfrac{\partial \xi_i}{\partial X_i} = 0$. The proper incompressibility equation $\nabla \cdot \underline{\xi} = \dfrac{\partial \xi_i}{\partial x_i} = 0$ is only approximately satisfied, at first order in $\|\nabla_0 \underline{\xi}\|$.

On the same domain Ω^S, we are trying to enforce, through the same no-slip boundary condition, two different "incompressibility"constraints: the solid incompressibility expressed with the reference state derivative and the fictitious fluid incompressibility constraint. We thus need to take in account the slight compressibility of the solid in order to strictly satisfy the no-slip condition. We need to add, within the virtual flow, a source term whose flow rate corresponds to the expansion of the structure.

In both the fluid and the solid, the pressure is now defined within an arbitrary constant. So, the pressure at infinity cannot be used as a criterion any more. Moreover, in our case, we do not need any additional criteria: S_0 must be fixed so that the two incompressibility rules can be both simultaneously satisfied. Hence, we want to find S_0 such that the flux through the boundary is the same for the fluid and for the solid:

$$\int_{\Gamma^{FSI}} \underline{u} \cdot \underline{n}^{S \to F} = \int_{\Gamma^{FSI}} \dot{\underline{\xi}} \cdot \underline{n}^{S \to F} \tag{A.11}$$

Using Gauss's theorem, the left hand side is shown to be simply S_0. The right hand side can be evaluated using the finite element discretization of $\underline{\xi}$:

$$\begin{aligned} S_0 = \ \mathcal{Q}^S \dot{\xi} \qquad \text{with} \quad \mathcal{Q}^S_{Ii} &= \int_{\Gamma^{FSI}(t)} \underline{N}^{\xi}_{Ii} \cdot \underline{n}^{S \to F} d\Gamma \\ &= \int_{\Gamma_0^{FSI}} N^{\xi}_{Ii} \ n_i^{S \to F} \left(\frac{d\Gamma(t)}{d\Gamma_0} \right) d\Gamma_0 \end{aligned} \tag{A.12}$$

Hence, using previous results (A.7), (A.9), (A.10) and (A.12), we obtain the formulation to express q_{irr}:

$$q_{irr} = \left(\mathcal{Q}^S \dot{\xi} \right) \ \mathcal{G} \ \Phi \qquad \text{with} \quad \Phi(t) = h_F^2 \left[g * \delta_{h_F} \big(\ \underline{x}_{center}(t) - \underline{x} \ \big) \right] \tag{A.13}$$

System (A.6) can then be re-written:

$$\begin{bmatrix} \mathbb{I} & & \\ & \cdot & \\ & & \cdot \end{bmatrix} \begin{bmatrix} \dot{\gamma} \\ \cdot \\ \cdot \end{bmatrix} + \begin{bmatrix} \beta S\Lambda S & -\,{}^t(\mathcal{E}_D\mathcal{C}) & \rho_0^S\,{}^t(\mathcal{E}\mathcal{C}) \\ \mathcal{E}_D\mathcal{C}S\Lambda^{-1}S & \cdot & \\ \mathcal{E}\ \mathcal{C}S\Lambda^{-1}S & & \cdot \end{bmatrix} \begin{bmatrix} \gamma \\ \tau_D^F \\ \tau \end{bmatrix}$$

$$= \begin{bmatrix} {}^t\mathcal{C}\big(\ h^F\ b^F - \mathcal{N}^F(q) + \ {}^t\mathcal{E}_N\tau_N^F\big) \\ h_F\ \mathcal{E}_D u_D - \Big(\mathcal{Q}^S\dot{\xi}\Big)\,\mathcal{E}_D\mathcal{G}\Phi - \mathcal{E}_D q_{uniform} \\ -\,{}^t\mathcal{T}^S\dot{\xi}\ -\ \Big(\mathcal{Q}^S\dot{\xi}\Big)\,\mathcal{E}\ \mathcal{G}\Phi - \mathcal{E}\ q_{uniform} \end{bmatrix} \quad \text{(A.14)}$$

This system is a modified formulation of (2.85). The additional terms, linearly dependant of $\dot{\xi}$ can easily be treated implicitly in the global coupled system.

APPENDIX B

Theoretical solution for vibrational modes of immersed circular disk

We describe in this appendix the derivation of the theoretical natural modes of vibration of the coupled system.

The solid reference state domain is defined in polar coordinates by $|\underline{x}| < R_0$.
The fluid is, at rest, defined on the remaining part of the plan: $|\underline{x}| > R_0$.

Consider our system disturbed from equilibrium by a small perturbation (initial condition).

At first order, the advective term in the Navier-Stokes equation (2.18) can be neglected. Thus, we have to solved the following linear system, where ω and s are the vorticity and the streamfunction of the 2D incompressible flow:

$$\left(\partial_t - \frac{1}{Re}\nabla^2\right)\omega(\underline{x},t) = 0 \qquad \forall \underline{x} : |\underline{x}| > R_0 \tag{B.1}$$

$$\nabla^2 \;\; s(\underline{x},t) = -\omega(\underline{x},t) \qquad \forall \underline{x} : |\underline{x}| > R_0 \tag{B.2}$$

$$\underline{u}(\underline{x},t) = \nabla \times s(\underline{x},t) \qquad \forall \underline{x} : |\underline{x}| > R_0 \tag{B.3}$$

$$\nabla p^F(\underline{x},t) = -\nabla \times \left(\dot{s} + \frac{1}{Re}\omega\right) \qquad \forall \underline{x} : |\underline{x}| > R_0 \tag{B.4}$$

Similarly for the 2D incompressible solid, define a vorticity-like and a streamfunction-like

fields ν and c such that the structure is subject to:

$$\left(\partial_{tt}^2 - \mu^s \ \nabla^2\right) \nu(\underline{x},t) = 0 \qquad \forall \underline{x} : |\underline{x}| < R_0 \tag{B.5}$$

$$\nabla^2 \ \ c(\underline{x},t) = -\nu(\underline{x},t) \qquad \forall \underline{x} : |\underline{x}| < R_0 \tag{B.6}$$

$$\underline{\xi}(\underline{x},t) = \nabla \times c(\underline{x},t) \qquad \forall \underline{x} : |\underline{x}| < R_0 \tag{B.7}$$

$$\nabla p^S(\underline{x},t) = -\nabla \times \left(\ddot{c} + \mu^S \nu\right) \qquad \forall \underline{x} : |\underline{x}| < R_0 \tag{B.8}$$

At first order, current and reference coordinates can be identified in the expression of any solid perturbation field $f \in \{\underline{\xi}, p^S, c, \nu\}$:

$$f(\underline{x},t) = f\left(\underline{X} + \underline{\xi}(\underline{X},t), t\right) \approx f(\underline{X},t) \tag{B.9}$$

$$\nabla_0 f = \frac{\partial f}{\partial \underline{X}} = \frac{\partial \underline{x}}{\partial \underline{X}} \frac{\partial f}{\partial \underline{x}} = \left(\underline{\underline{I}} + \frac{\partial \underline{\xi}}{\partial \underline{X}}\right) \nabla f \approx \nabla f \tag{B.10}$$

Solutions of the form $\omega(r,\theta,t) = \Re\left[\hat{\omega}(r)\ e^{i\sigma t}\right]\sin(m\theta)$ and $\nu(r,\theta,t) = \Re\left[\hat{\nu}(r)\ e^{i\sigma t}\right]\sin(m\theta)$ are investigated. $\Re$ stands for the real part operator. σ is the complex pulsation (its real part is the current pulsation and its imaginary part characterizes the dumping) and m is the angular mode. σ and m are the two eigenvalues. In solutions below, we denotes by J the Bessel functions of the first kind and by K the modified Bessel functions of the second kind.

$$\exists (B,D) \in \mathbb{C}^2 : \quad \begin{cases} \omega(r,\theta,t) &= \Re\Big[\quad B\ K_m(\kappa r) \quad\quad\quad\quad e^{i\sigma t}\Big]\sin(m\theta) \\ s(r,\theta,t) &= \Re\Big[\Big(\quad -\dfrac{B}{\kappa^2} K_m(\kappa r) + \quad D\ r^{-m} \quad \Big)e^{i\sigma t}\Big]\sin(m\theta) \\ u_r(r,\theta,t) &= \Re\Big[\Big(-m\ \dfrac{B}{\kappa^2 r} K_m(\kappa r) + m\ D\ r^{-m-1}\Big)e^{i\sigma t}\Big]\cos(m\theta) \\ u_\theta(r,\theta,t) &= \Re\Big[\Big(\quad \dfrac{B}{\kappa} K_m'(\kappa r) + m\ D\ r^{-m-1}\Big)e^{i\sigma t}\Big]\sin(m\theta) \\ p^F(r,\theta,t) &= \Re\Big[\Big(\quad\quad\quad\quad\quad i\sigma\ D\ r^{-m} \quad \Big)e^{i\sigma t}\Big]\cos(m\theta) \end{cases} \tag{B.11}$$

with $\kappa = \sqrt{i\sigma Re}$ (B.12)

$$\exists (A,C) \in \mathbb{C}^2 : \quad \begin{cases} \nu(r,\theta,t) &= \Re\Big[\quad A\ J_m(\lambda r) \quad\quad\quad\quad\quad\quad\quad\quad e^{i\sigma t}\Big] \sin(m\theta) \\ c(r,\theta,t) &= \Re\Big[\big(\quad \dfrac{A}{\lambda^2} J_m(\lambda r) + \quad C\ r^m \quad \big) e^{i\sigma t}\Big] \sin(m\theta) \\ \xi_r(r,\theta,t) &= \Re\Big[\big(m\ \dfrac{A}{\lambda^2 r} J_m(\lambda r) + m\ C\ r^{m-1} \big) e^{i\sigma t}\Big] \cos(m\theta) \\ \xi_\theta(r,\theta,t) &= \Re\Big[\big(\quad -\dfrac{A}{\lambda} J'_m(\lambda r) - m\ C\ r^{m-1} \big) e^{i\sigma t}\Big] \sin(m\theta) \\ p^S(r,\theta,t) &= \Re\Big[\big(\quad\quad\quad\quad\quad\quad \sigma^2\ C\ r^m \quad \big) e^{i\sigma t}\Big] \cos(m\theta) \end{cases} \tag{B.13}$$

$$\text{with } \lambda = \sqrt{\frac{\sigma^2}{\mu^S}} \tag{B.14}$$

The boundary conditions between fluid and solid are the following, where ρ_0^S stands for the solid-over-fluid density ratio:

$$\dot{\underline{\xi}}(R_0,\theta,t) = \underline{u}(R_0,\theta,t) \qquad \forall (\theta,t) \tag{B.15}$$

$$\rho_0^S \ \ \underline{\underline{P}}(R_0,\theta,t) \cdot \underline{e}_r = \underline{\underline{\sigma}}(R_0,\theta,t) \cdot \underline{e}_r \qquad \forall (\theta,t) \tag{B.16}$$

Thanks to the two no-slip (scalar) equations (B.15), the four complex coefficients A, B, C and D can be expressed in terms of the two independent parameters γ and δ, defined as follows:

$$\begin{cases} \dot{\xi}_r(R_0,\theta,t) = u_r(R_0,\theta,t) = \Re\left[(\delta+\gamma)e^{i\sigma t}\right]\cos(m\theta) \\ \dot{\xi}_\theta(R_0,\theta,t) = u_\theta(R_0,\theta,t) = \Re\left[(\delta-\gamma)e^{i\sigma t}\right]\sin(m\theta) \end{cases} \tag{B.17}$$

$$A = \frac{1}{i\sigma} \frac{2\ \lambda}{J_{m+1}(\lambda R_0)}\ \delta \qquad\qquad C = \frac{1}{i\sigma} \frac{1}{m R_0^{m-1}} \left(\gamma - \frac{J_{m-1}(\lambda R_0)}{J_{m+1}(\lambda R_0)}\ \delta \right) \tag{B.18}$$

$$B = \frac{2\ \kappa}{K_{m-1}(\kappa R_0)}\ \gamma \qquad\qquad D = \frac{R_0^{m+1}}{m} \left(\delta + \frac{K_{m+1}(\kappa R_0)}{K_{m-1}(\kappa R_0)}\ \gamma \right) \tag{B.19}$$

The formula obtained by Zhang & Eldredge [ZE09] is recovered by fixing $m = 2$, $\sigma = \Omega$, $\gamma = 0$ and $\delta = a_0\Omega$. Note that the coefficient κ has not been defined similarly.

We also want to satisfy the stress balance (B.16). Stresses in the fluid and in the solid domains are given below.

$$\begin{aligned}\sigma_{rr}(r,\theta,t) &= 2\frac{i\sigma}{\kappa^2}\partial_r u_r - p^F \\ &= \Re\left[i\sigma\frac{r}{m}\begin{pmatrix} \left(\begin{array}{l}\dfrac{2m(m+1)}{\kappa^2 r^2}K_{m+1}(\kappa r) \\ +\dfrac{2m(m-1)}{\kappa^2 r^2}K_{m-1}(\kappa r)\end{array}\right)\dfrac{B}{2\kappa} \\ -\Big(\dfrac{2m(m+1)}{\kappa^2 r^2}+1\Big)\dfrac{mD}{r^{m+1}}\end{pmatrix} e^{i\sigma t}\right]\cos(m\theta)\end{aligned} \tag{B.20}$$

$$\begin{aligned}\sigma_{r\theta}(r,\theta,t) &= \frac{i\sigma}{\kappa^2}\left(\partial_r u_\theta + \frac{1}{r}(\partial_\theta u_r - u_\theta)\right) \\ &= \Re\left[i\sigma\frac{r}{m}\begin{pmatrix} \left(\begin{array}{l}\left(1+\dfrac{2m(m+1)}{\kappa^2 r^2}\right)K_{m+1}(\kappa r) \\ -\left(1+\dfrac{2m(m-1)}{\kappa^2 r^2}\right)K_{m-1}(\kappa r)\end{array}\right)\dfrac{B}{2\kappa} \\ -\dfrac{2m(m+1)}{\kappa^2 r^2}\dfrac{mD}{r^{m+1}}\end{pmatrix} e^{i\sigma t}\right]\sin(m\theta)\end{aligned} \tag{B.21}$$

$$\begin{aligned}P_{rr}(r,\theta,t) &= 2\frac{\sigma^2}{\lambda^2}\partial_r \xi_r - p^S \\ &= \Re\left[\sigma^2\frac{r}{m}\begin{pmatrix} \left(\begin{array}{l}\dfrac{2m(m-1)}{\lambda^2 r^2}J_{m-1}(\lambda r) \\ -\dfrac{2m(m+1)}{\lambda^2 r^2}J_{m+1}(\lambda r)\end{array}\right)\dfrac{A}{2\lambda} \\ +\Big(\dfrac{2m(m-1)}{\lambda^2 r^2}-1\Big)mCr^{m-1}\end{pmatrix} e^{i\sigma t}\right]\cos(m\theta)\end{aligned} \tag{B.22}$$

$$\begin{aligned}P_{r\theta}(r,\theta,t) &= \frac{\sigma^2}{\lambda^2}\left(\partial_r \xi_\theta + \frac{1}{r}(\partial_\theta \xi_r - \xi_\theta)\right) \\ &= \Re\left[\sigma^2\frac{r}{m}\begin{pmatrix} \left(\begin{array}{l}\left(1-\dfrac{2m(m-1)}{\lambda^2 r^2}\right)J_{m-1}(\lambda r) \\ +\left(1-\dfrac{2m(m+1)}{\lambda^2 r^2}\right)J_{m+1}(\lambda r)\end{array}\right)\dfrac{A}{2\lambda} \\ -\dfrac{2m(m-1)}{\lambda^2 r^2}mCr^{m-1}\end{pmatrix} e^{i\sigma t}\right]\sin(m\theta)\end{aligned} \tag{B.23}$$

Substitute with the values (B.18)-(B.19) of A, B, C and D that match the no-slip conditions, and evaluate at the boundary location $r = R_0$:

$$\sigma_{rr}(R_0,\theta,t) = \Re\left[i\sigma\frac{R_0}{m}\left(\begin{array}{r} \left(\dfrac{2m(m-1)}{\kappa^2R_0^2} - \dfrac{K_{m+1}(\kappa R_0)}{K_{m-1}(\kappa R_0)}\right)\gamma \\ -\left(\dfrac{2m(m+1)}{\kappa^2R_0^2}+1\right)\delta \end{array}\right) e^{i\sigma t}\right]\cos(m\theta) \tag{B.24}$$

$$\sigma_{r\theta}(R_0,\theta,t) = \Re\left[i\sigma\frac{R_0}{m}\left(\begin{array}{r} \left(\dfrac{K_{m+1}(\kappa R_0)}{K_{m-1}(\kappa R_0)} - \dfrac{2m(m-1)}{\kappa^2R_0^2} - 1\right)\gamma \\ -\left(\dfrac{2m(m+1)}{\kappa^2R_0^2}\right)\delta \end{array}\right) e^{i\sigma t}\right]\sin(m\theta) \tag{B.25}$$

$$P_{rr}(R_0,\theta,t) = \Re\left[i\sigma\frac{R_0}{m}\left(\begin{array}{r} \left(\dfrac{2m(m+1)}{\lambda^2R_0^2} - \dfrac{J_{m-1}(\lambda R_0)}{J_{m+1}(\lambda R_0)}\right)\delta \\ -\left(\dfrac{2m(m-1)}{\lambda^2R_0^2}-1\right)\gamma \end{array}\right) e^{i\sigma t}\right]\cos(m\theta) \tag{B.26}$$

$$P_{r\theta}(R_0,\theta,t) = \Re\left[i\sigma\frac{R_0}{m}\left(\begin{array}{r} \left(\dfrac{J_{m-1}(\lambda R_0)}{J_{m+1}(\lambda R_0)} - \dfrac{2m(m+1)}{\lambda^2R_0^2} + 1\right)\delta \\ +\left(\dfrac{2m(m-1)}{\lambda^2R_0^2}\right)\gamma \end{array}\right) e^{i\sigma t}\right]\sin(m\theta) \tag{B.27}$$

For given m, R_0 and ρ_0^S, we have to find the values of δ, γ and σ (also involved in the definitions (B.12)-(B.14) of κ and λ) such that the stress balance (B.16) is satisfied.

Re	ρ_0^S	δ/γ	σ
200	0.1	$1.3851\ e^{-2.8403i}$	$2.6649 \times (1 + 1.0335\ 10^{+0}\ i)$
200	1.0	$27.233\ e^{-1.5373i}$	$8.4294 \times (1 + 2.1195\ 10^{-2}\ i)$
200	10	$0.4486\ e^{+3.1147i}$	$4.6130 \times (1 + 2.0585\ 10^{-3}\ i)$
40	1.0	$5.8967\ e^{-1.4111i}$	$8.7866 \times (1 + 1.0629\ 10^{-1}\ i)$
1000	1.0	$135.43\ e^{-1.5645i}$	$8.4045 \times (1 + 3.9968\ 10^{-3}\ i)$

Table B.1: *Eigenvalues m and σ for some particular entries Re and ρ_0^S.*

References

[All07] G. Allaire. *Numerical Analysis and Optimization: An Introduction to Mathematical Modelling and Numerical Simulation (Numerical Mathematics and Scientific Computation)*. Oxford University Press, 2007.

[Ben92] D. J. Benson. "Computational methods in Lagrangian and Eulerian hydrocodes." *Comput. Methods Appl. Mech. Eng.*, **99**(2-3):235–394, September 1992.

[BM00] W. K. Belytschko and B. Moran. *Nonlinear Finite Elements for Continua and Structures*. Wiley, New York, 2000.

[CGN05] P. Causin, J. F. Gerbeau, and F. Nobile. "Added-mass effect in the design of partitioned algorithms for fluid-structure problems." *Computer Methods in Applied Mechanics and Engineering*, **194**(42-44):4506–4527, 2005.

[CGP02] W. Chang, F. Giraldo, and B. Perot. "Analysis of an Exact Fractional Step Method." *Journal of Computational Physics*, **180**(1):183 – 199, 2002.

[Cho73] A. J. Chorin. "Numerical study of slightly viscous flow." *Journal of Fluid Mechanics*, **57**:785–796, Mar 1973.

[CK00] G.-H. Cottet and P. Koumoutsakos. *Vortex methods - theory and practice.* Cambridge University Press, 2000.

[CMP02] R. D. Cook, D. S. Malkus, M. E. Plesha, and R. J. Witt. *Concepts and applications of finite element analysis*. John Wiley and Sons. Inc., fourth edition, 2002.

[CT08] T. Colonius and K. Taira. "A fast immersed boundary method using a nullspace approach and multi-domain far-field boundary conditions." *Computer Methods in Applied Mechanics and Engineering*, **197**(25–28):2131 – 2146, 2008.

[Eld08] J. D. Eldredge. "Dynamically coupled fluid-body interactions in vorticity-based numerical simulations." *Journal of Computational Physics*, **227**(21):9170–9194, Nov 2008.

[FAM99] R. P. Fedkiw, T. Aslam, B. Merriman, and S. Osher. "A non-oscillatory Eulerian approach to interfaces in multimaterial flows (the ghost fluid method)." *Journal of Computational Physics*, **152**(2):457–492, Jul 1999.

[Fed02] R. P. Fedkiw. "Coupling an Eulerian fluid calculation to a Lagrangian solid calculation with the ghost fluid method." *Journal of Computational Physics*, **175**(1):200–224, Jan 2002.

[FL93] C. Farhat and M. Lesoinne. "Automatic partitioning of unstructured meshes for the parallel solution of problems in computational mechanics." *International Journal For Numerical Methods in Engineering*, **36**(5):745–, Mar 1993.

[GKF11] J. T. Gretarsson, N. Kwatra, and R. Fedkiw. "Numerically stable fluid-structure interactions between compressible flow and solid structures." *Journal of Computational Physics*, **230**(8):3062–3084, Apr 2011.

[GM77] R. A. Gingold and J. J. Monaghan. "Smoothed particle hydrodynamics - Theory and application to non-spherical stars." *Monthly Notices of the Royal Astronomical Society*, **181**(2):375–389, 1977.

[HK08] S. E. Hieber and P. Koumoutsakos. "An immersed boundary method for smoothed particle hydrodynamics of self-propelled swimmers." *Journal of Computational Physics*, **227**(19):8636–8654, Oct 2008.

[HPZ01] H. H. Hu, N. A. Patankar, and M. Y. Zhu. "Direct numerical simulations of fluid-solid systems using the arbitrary Lagrangian-Eulerian technique." *Journal of Computational Physics*, **169**(2):427–462, May 2001.

[HW98] H. Han and X. Wu. "A New Mixed Finite Element Formulation and the MAC Method for the Stokes Equations." *SIAM Journal of Numerical Analysis*, **35**(2):560–571, April 1998.

[JH04] X. M. Jiao and M. T. Heath. "Common-refinement-based data transfer between non-matching meshes in multiphysics simulations." *International Journal For Numerical Methods in Engineering*, **61**(14):2402–2427, Dec 2004.

[KRN12] K. Kamrin, C. H. Rycroft, and J.-C. Nave. "Reference map technique for finite-strain elasticity and fluid-solid interaction." *Journal of the Mechanics and Physics of Solids*, **60**(11):1952–1969, Nov 2012.

[LCB06] A. Legay, J. Chessa, and T. Belytschko. "An Eulerian-Lagrangian method for fluid-structure interaction based on level sets." *Computer Methods in Applied Mechanics and Engineering*, **195**(17-18):2070–2087, 2006.

[Leo80] A. Leonard. "Vortex methods for flow simulation." *Journal of Computational Physics*, **37**(3):289–335, 1980.

[LKX06] T. G. Liu, B. C. Khoo, and W. F. Xie. "The modified Ghost Fluid Method as applied to extreme fluid-structure interaction in the presence of cavitation." *Communications in Computational Physics*, **1**(5):898–919, Oct 2006.

[LL94] R. J. Leveque and Z. L. Li. "The Immersed Interface Method for Elliptic Equations with Discontinuous Coefficients and Singular Sources." *SIAM Journal on Numerical Analysis*, **31**(4):1019–1044, Aug 1994.

[LL97] R. J. Leveque and Z. L. Li. "Immersed interface methods for Stokes flow with elastic boundaries or surface tension." *SIAM Journal on Scientific Computing*, **18**(3):709–735, May 1997.

[LLF06] W. K. Liu, Y. L. Liu, D. Farrell, L. Zhang, X. S. Wang, Y. Fukui, N. Patankar, Y. J. Zhang, C. Bajaj, J. Lee, J. H. Hong, X. Y. Chen, and H. Y. Hsu. "Immersed finite element method and its applications to biological systems." *Computer Methods in Applied Mechanics and Engineering*, **195**(13-16):1722–1749, 2006.

[LMZ08] H. Luo, R. Mittal, X. Zheng, S. A. Bielamowicz, R. J. Walsh, and J. K. Hahn. "An immersed-boundary method for flow-structure interaction in biological systems with application to phonation." *Journal of Computational Physics*, **227**(22):9303–9332, Nov 2008.

[MI05] R. Mittal and G. Iaccarino. "Immersed boundary methods." *Annual Review of Fluid Mechanics*, **37**:239–261, 2005.

[Per93] J. B. Perot. "An Analysis of the Fractional Step Method." *Journal of Computational Physics*, **108**(1):51 – 58, 1993.

[Pes72] C. S. Peskin. "Flow patterns around heart valves: A numerical method." *Journal of Computational Physics*, **10**(2):252–, 1972.

[Pes02] C. S. Peskin. "The immersed boundary method." *Acta Numerica*, **11**:479–517, 2002.

[RPB99] A. M. Roma, C. S. Peskin, and M. J. Berger. "An adaptive version of the immersed boundary method." *Journal of Computational Physics*, **153**(2):509–534, Aug 1999.

[RSG08] A. Robinson-Mosher, T. Shinar, J. Gretarsson, J. Su, and R. Fedkiw. "Two-way coupling of fluids to rigid and deformable solids and shells." *ACM Transactions on Graphics*, **27**(3):46, Aug 2008.

[SW00] J. A. Sethian and A. Wiegmann. "Structural boundary design via level set and immersed interface methods." *Journal of Computational Physics*, **163**(2):489–528, Sep 2000.

[TC07] K. Taira and T. Colonius. "The immersed boundary method: A projection approach." *Journal of Computational Physics*, **225**(2):2118 – 2137, 2007.

[UMR01] H. S. Udaykumar, R. Mittal, P. Rampunggoon, and A. Khanna. "A sharp interface cartesian grid method for simulating flows with complex moving boundaries." *Journal of Computational Physics*, **174**(1):345–380, Nov 2001.

[WB09] H. Wang and T. Belytschko. "Fluid-structure interaction by the discontinuous-Galerkin method for large deformations." *International Journal For Numerical Methods in Engineering*, **77**(1):30–49, Jan 2009.

[WL04] X. D. Wang and W. K. Liu. "Extended immersed boundary method using FEM and RKPM." *Computer Methods in Applied Mechanics and Engineering*, **193**(12-14):1305–1321, 2004.

[ZE09] L. Zhang and J. Eldredge. "A viscous vortex particle method for deforming bodies with application to biolocomotion." *International Journal for Numerical Methods in Fluids*, **59**(12):1299–1320, 2009.

[ZWH12] Y. Zhu, Y. Wang, J. Hellrung, A. Cantarero, E. Sifakis, and J. M. Teran. "A second-order virtual node algorithm for nearly incompressible linear elasticity in irregular domains." *J. Comput. Physics*, **231**(21):7092–7117, 2012.